Heliyon 9 (2023) e20864

Contents lists available at ScienceDirect

Heliyon

journal homepage: www.cell.com/heliyon

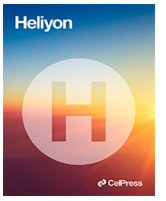

# Experimental and analytical investigation on forced and free vibration of sandwich structures with reinforced composite faces in an acidic environment

Farshad Rahmani [a], Reza Barbaz-Isfahani [a,b], Saeed Saber-Samandari [b,c,*], Manouchehr Salehi [a]

[a] Department of Mechanical Engineering, Amirkabir University of Technology, Tehran, Iran
[b] New Technologies Research Center, Amirkabir University of Technology, Tehran, Iran
[c] Composites Research Laboratory (CRLab), Amirkabir University of Technology, Tehran, Iran

ARTICLE INFO

*Keywords:*
Sandwich composite panel
Nanoparticles
Vibration
Finite element modeling
Acidic environment

ABSTRACT

The main objective of this study is to investigate the impact of nanoparticles as reinforcement material on the vibrational behavior of sandwich structures in an acidic medium. The glass fiber reinforced polymer (GFRP) faces were fabricated with and without the addition of 3 wt% nanoclay and nanosilica to determine the mechanical behaviors of the GFRP faces in the presence of an acidic medium. The obtained results showed adding 3 wt% of nanoclay caused better durability and less mass variation of composite specimens in sulfuric acid. The "Coefficient of acidic immersion expansion" ($\beta^{acid}$) is determined by measuring the length and mass variation of GFRP specimens in the immersion, and applied to low order piecewise shear deformation theory (LOPSDT) for the first time; Also the frequency results of LOPSDT have been shown good agreement in validation with the ANSYS numerical solution. It is shown that acidic environment reduces the frequency of the first mode of sandwich plates with reinforced face by 3 wt% nanosilica, and nanoclay has increased by 6.81 % and 4.66 %, respectively. This study indicates after one month of immersion, the natural frequency of the sandwich with pure, and 3 wt% nanoclay reduces about 1 %, and the natural frequency of the sandwich with the faces reinforced with 3 wt% nanosilica reduces by more than 3 %; Moreover, the frequency of forced vibrations, caused by acidic immersion expansion, was improved significantly by 10.04 % and 6.54 % in the first mode by incorporating 3 wt% of nanoclay, and nanosilica into the faces of the sandwich in one month of immersion compared to the sandwich with pure faces.

## 1. Introduction

Sandwich panels are used in various industries in terms of their lightweight, and resistance to external effects [1–4]. An acidic environment is known as a destructive environment that changes the mechanical properties, and dynamic characteristics of structures; Therefore, the analysis of structures, such as storage tanks and desulfurization pipelines and their vibrations in the chemical and corrosive industries requires a comprehensive study [5–9]. Based on a review of prior research, it is evident that researchers have

* Corresponding author. New Technologies Research Center, Amirkabir University of Technology, Tehran, Iran.
*E-mail address:* saeedss@aut.ac.ir (S. Saber-Samandari).

https://doi.org/10.1016/j.heliyon.2023.e20864
Received 30 April 2023; Received in revised form 27 September 2023; Accepted 9 October 2023
Available online 10 October 2023

shown a keen interest in exploring the behavior of different materials and structures under mechanical loading [10–14]. Such investigations can provide valuable insights for structural design by shedding light on how materials behave under various loading conditions [15–19]. Notably, the study of structural behavior under vibrational loading has garnered considerable attention from researchers, given the crucial role that vibrations play in real-world structural loading conditions [20]. In order to mitigate the deleterious effects of acidic environments on structures subjected to various forces, it is imperative to have a thorough understanding of the medium and the design of the structures, and to implement appropriate preventive and remedial measures [21–24]. In industries involved in pipelines and sulfuric acid production, sulfurization and heat exchangers are particularly vulnerable to environmental corrosion resulting from exposure to sulfur and sulfuric acid [25]. Furthermore, structures operating in highly acidic and low-pH environments are often subject to significant deterioration, resulting in diminished mechanical and physical properties [26].

For the mechanical properties of composite structure, and its vibration behavior in the acidic medium, several factors are involved [27,28]. Based on the previous literature, fibers and adding clay and silica nanoparticles played an important role due to their chemical properties, manufacturing process, particle morphology, and the type of bonding of nanoparticles to polymers [29–35].

Thus, many studies on the effect of adding nanoparticles in destructive and acidic environments were studied based on the experimental tests [36,37].

In the literature, studying the vibrations of sandwich structures in different environments was studied. However, few studies were conducted in the field of strengthening the sandwich structure with nanoparticles, and comparing them to improve the vibration behavior and forced vibrations under environmental pre-stress based on the experimental tests and analytical and numerical solutions. Hamami et al. [38] evaluated the durability, and environmental degradation of glass-vinyl ester composites in high temperature, humid environments, seawater, and corrosive fluids. They performed the experiments on the composites using three-point bending test; it was observed that, in corrosive fluids, by increasing the fluid concentration of medium, and the immersion time, the performance of composite specimens drastically changed; Moreover, after a longer immersion period, the swellings grow which cause the composites to fail. Kamal et al. [37] investigated the impact of both alkaline and acidic solutions on the mechanical properties of polymer composite materials. Hardness, tensile properties, and effect strength of composite specimen (glass/kevlar) reinforced with the nanosilica particles before and after immersion in HCl and NaOH solutions were studied, and regardless of the solution, hardness, tensile, and effect resistance decreased by increasing immersion time. Tanks et al. [39] conducted an experiment to investigate the effect of water and sulfuric acid solutions on the strength of plain-weave laminates composed of *C*-glass and amine-cured epoxy. The outcomes revealed that both solutions damage the fibers, with sulfuric acid having a more severe impact. Specifically, sulfuric acid increases the absorption and saturation uptake of water in the structures, leading to a notable reduction in the mechanical properties. Reddy et al. [40] evaluted the impact of adding nanoparticles to glass/epoxy laminates by changing the loading of nanoclay from 0 wt % to 12 wt%, and subjected them to low velocity impact energy. In their study, by increasing the effect energy to 110 J, the energy absorption of nanocomposite laminates was improved by 37 % compared to the laminate without nanoparticles; Therefore, incorporated composite specimen with 9 wt% nanoclay showed a more favorable performance in terms of the energy absorption and displacement. Chang et al. [41] investigated the mechanical behavior of two types of fiber-reinforced polymers, namely epoxy and vinyl ester resin, which were enhanced with various amounts of nanosilica (1, 2, 3, and 4 wt%). The study found that the optimal improvement in mechanical properties was achieved with a nanoparticle content of 3 wt%. Specifically, the inclusion of nanoparticles led to a 26 % increase in tensile strength, a 6 % increase in bending resistance, and a 49 % increase in impact resistance of the epoxy resin compared to the resin without nanoparticles. Based on a review of previous studies, it is clear that adding nanoparticles can have a beneficial effect on the properties of various materials [42–44]. The phenomenon has been witnessed in polymer and fiber-reinforced composite materials, which have undergone improvements through the incorporation of diverse nanoparticles [45–47]. The bolstered mechanical characteristics can be ascribed to the superior mechanical properties possessed by the reinforcing nanoparticles [48–51].

Alsaadi et al. [52] carried out an experimental investigation to examine the influence of nanoparticles (specifically nano-silica) on the mechanical properties of hybrid composites comprising woven fibers, carbon, Kevlar, and epoxy. The study focused on analyzing the tensile strength, vibration characteristics, and damping properties of the composites. The results revealed notable changes when nano-silica was incorporated into the epoxy resin. Specifically, a significant increase of 20.5 % in the natural frequency of the composites was observed when the nano-silica content reached 0.5 wt%. Moreover, the researchers noted enhancements in both flexural and tensile strength upon the introduction of nano-silica into the composites. This improvement was attributed to the effective bonding between the nano-silica particles and the epoxy/fiber system, resulting in enhanced load transfer between the particles and the matrix. Senthamaraikannan et al. [53] conducted a study on the free vibration characteristics of carbon fiber reinforced composite beams, which incorporated a blend of nanosilica and carboxyl-terminated butadiene acrilonitrile copolymer particles of micro size in an epoxy matrix. The results indicated that incorporating both nano-sized silica particles and micro-sized particles led to an enhancement in the damping performance of the composite beams, along with an improvement in their flexural rigidity. These results demonstrate that the use of such hybrid composites can be highly effective in structural applications.

Wiwat et al. [54], by studying acid penetration in the reinforced composite with nanoclay, stated that nanoclay, and its weight percentage for the nanocomposites have an effective performance against sulfuric acid. It was stated that the homogeneity of particles is vital to make the specimens; besides, the layered nanoclays are effective to stabilize the movement of polymer and prevent the rapid penetration of $(SO_4^{2-})$ ions into the matrix. Gitiara et al. [55] conducted a study to investigate the impact behaviors of GFRP reinforced by nanoclay (NC) and nanosilica (NP) after immersion in sulfuric acid for 0, 1, and 3 months. The findings indicate that GFRP reinforced with nanoclay exhibited better low-velocity impact behavior. Specifically, the addition of 5 wt% of nanoclay resulted in a 15.72 % increase in impact force and a 5.26 % decrease in displacement. Li et al. [56] developed mathematical models that incorporate both low-order and high-order piecewise shear deformation to account for the in-plane rigidity and transverse shear rigidity of sandwich

panels' core and faces. These models were compared against finite element analysis, demonstrating their effectiveness in accurately predicting the frequency equation for a simply supported rectangular sandwich panel. Furthermore, the researchers utilized the derived theoretical solution to analyze the thermal post-buckling and free vibration of a sandwich beam. By applying the principle of virtual work, nonlinear equations were obtained for a sandwich beam with a soft core. The study also investigated the vibration analysis of a post-buckling sandwich beam and observed that, at a critical temperature, the beam exhibited a sudden increase in deformation, resulting in loss of stability [57]. In other research, the effects of vibration, and buckling of sandwich structures in terms of the thermal loads and forced vibrations were studied [58,59].

Upon reviewing the existing literature, it became apparent that limited research has been conducted on the impact of silica and clay nanoparticles on the free and forced vibrations of sandwich plates reinforced with GFRP composite faces in acidic environments. As a result, this study aims to investigate the effect of incorporating 3 wt% of clay and silica nanoparticles on the strengthening of composite faces in a 5 % sulfuric acid solution. The hydrophobicity and hydrophilicity of the added nanoparticles are taken into consideration, and the effect of their incorporation on the mechanical behavior, weight, and length variation of GFRP composites in an acidic immersion is examined. The $\beta^{acid}$ is then determined to quantify this effect. Next, the equations of motion are derived to express the effect of the manufactured GFRP composite on the natural and forced frequencies of sandwich plates with a softcore immersed in 5 % sulfuric acid. The obtained natural and forced frequencies of the sandwich plates are then compared to finite element simulation results to validate the findings. Finally, the study compares the efficacy of adding nanosilica and nanoclay to GFRP faces and examines their impact in the sulfuric acid solution. The research gap identified in the previous studies underlines the significance and application of this study in the field of composite materials, particularly in acidic environments.

## 2. Experimental procedure

In order to investigate the impact of incorporating nanoparticles in strengthening the faces of sandwich structures, three types of GFRP composite faces were fabricated: pure composite, reinforced faced sheets with clay nanoparticles, and reinforced faced sheets with silica nanoparticles. The mechanical properties of these faces were tested, including their response to an acidic environment. The obtained properties will be utilized in the analytical solution of sandwich plate vibrations with a soft core.

### 2.1. Materials and fabrication method

To fabricate the composite specimens, *C*-glass material with a surface density of 600 g/m2 was obtained from Mytex Turkey. Epon 828 epoxy resin and its hardener, Deithvlenetriamine (DETA), in a ratio of 100:10 by weight, were purchased from Kumho P&B Chemicals. In this study, two different types of nanoparticles were utilized to enhance the mechanical properties of composite materials in acidic conditions. The first type consisted of clay nanoparticles (Cloisite 15A) supplied by Merck, Germany, with a plate diameter measuring 24.2 nm and a density of 1.77. The second type comprised spherical silica nanoparticles obtained from Tecnan nano-materials Co., Spain, with an average particle size ranging from 20 to 30 nm. Composite specimens were fabricated by

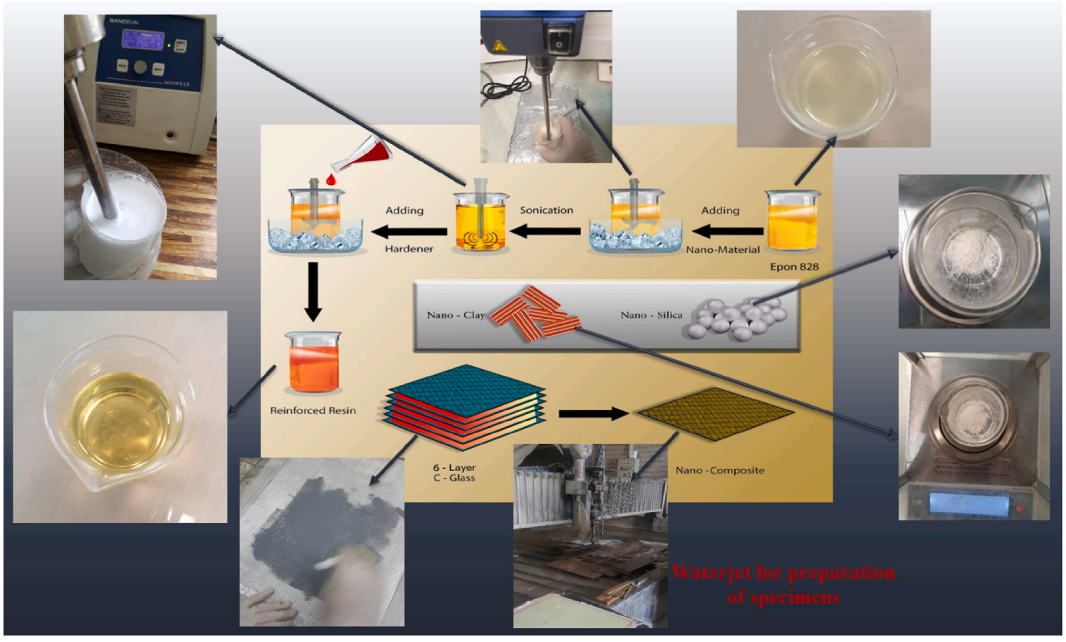


**Fig. 1.** A schematic representation of the fabrication process used to create the pure and nanocomposite specimens with 3 wt% of nanosilica (NS) and nanoclay(NC).

incorporating 3 wt% of both nanosilica and nanoclay into the pure composite material. The objective of this research was to investigate the impact of these additional nanoparticles on the mechanical properties of the composite materials under acidic conditions. To achieve this objective, the type of nanoparticles and their weight percentage were selected based on our prior research. However, it is important to note that the addition of a high concentration of nanoparticles may not necessarily result in a significant improvement in mechanical properties. In fact, the agglomeration of nanoparticles and insufficient degassing during the fabrication process may lead to a reduction in mechanical properties due to stress concentration within the samples. This can be attributed to the increase in viscosity of the resin due to the presence of high loading nanoparticles [60–62].

The fabrication process of composite specimens is shown in Fig. 1. As the schematic of fabrication process shows, first, 3 wt% of nanoclay or nanosilica was added into Epon 828 resin followed by mechanical mixing for 40 min and sonication for 35 min to well distribution of nanoparticles into the epoxy resin based on our previous study method [63–65]. Following the addition of the appropriate quantity of hardener to the pure epoxy resin and the epoxy resin filled with nanoparticles, the mixture underwent a degassing process in a vacuum oven for a duration of 20 min. This step aimed to eliminate any air pockets that may have formed during the mixing procedure. The composite sheets were fabricated using the hand layup method with six layers of *C*-glass woven fabric. The laminates were then cured under a pressure of 10 KPa at 25 °C for 24 h. Finally, specimens for characteristic testing were cut using a water-jet method.

### 2.2. Evaluation of mechanical properties of prepared composites in the acidic medium

The mechanical characteristics of the face specimens of the sandwich plate were evaluated through experimental testing following their immersion in a 5 % sulfuric acid solution for a duration of 30 days. According to the standard and our previous research [55], the immersion tests of specimens in the chemical environment are designed, and the elastic modulus, and weight and longitudinal variation of the GFRP composite faces are measured in 5 % sulfuric acid [66,67].

Tensile and shear elastic modulus of GFRP composite faces after 0 and 30 days of immersion was performed with SANTAM universal testing machine (UTM) based on ASTM D3039 and ASTM D3518 standards [68,69]; Furthermore, the density of fabricated faces before immersion was measured based on ISO 1183 standard [70].

The mechanical behaviors of three composite face specimens were experimentally determined, including pure GFRP composite and incorporated GFRP composites with 3 wt% of silica and clay nanoparticles. As anticipated, the mechanical properties of the immersed specimens were reduced as a result of exposure to the corrosive environment, as shown in Table 1.

To calculate the $\beta^{acid}$ of fabricated composites, length, and weight variations were measured in sulfuric acid. The longitudinal changes of specimens were similarly measured to a previous study reported by Refs. [71,72] with a profile projector of Nikon company in two directions. This instrument measures the length with a precision of 1 μm. Weight changes were measured with an accuracy of 0.001 g for each specimen. The ratio of length and weight changes of the fabricated composites is compared according to Eq. (1).

$$\text{ratio of weight variation} = \frac{M_{final} - M_{initial}}{M_{initial}} = \left(\frac{\Delta M}{M_0}\right)$$

$$\text{ratio of length variation} = \frac{L_{final} - L_{initial}}{L_{initial}} = \left(\frac{\Delta L}{L_0}\right) \tag{1}$$

The experiments of this research are different in the type of solution, the immersion time, and measuring devices, which were changed based on the conditions of project. After immersing the composites in sulfuric acid 5 %, in certain time intervals, the length of specimens was measured by the profile projector. To determine the weight changes, the composites were removed from the acid, and before measuring, specimens drying with a napkin.

The $\beta^{acid}$ is calculated according to Eq. (2) by determining the relative length and mass variation of specimens. Hence, the linear part of length and weight changes of GFRP composites was used to calculate $\beta^{acid}$, before their moisture saturation and about 30 days (See Fig. 2).

$$\left(\frac{\Delta L}{L_0}\right) \Big/ \left(\frac{\Delta M}{M_0}\right) = \beta^{acid} \tag{2}$$

The $\beta^{acid}$ of fabricated GFRP faces is presented in Table 1. Based on the results, $\beta^{acid}$ of the pure composite is higher than fabricated

**Table 1**
Mechanical properties of fabricated GFRP faces in 0 and 30 days of submerging in the sulfuric acid.

| Composites type | Immersion Time (day) | $E_1(GPa)$ | $E_2(GPa)$ | $G_{12}(GPa)$ | $v_{12}$ | $\rho\left(\frac{Kg}{m^3}\right)$ | $\beta_{xx}^{acid} = \beta_{yy}^{acid}$ |
|---|---|---|---|---|---|---|---|
| Pure composites | 0 | 10.61 | 10.61 | 3.69 | 0.266 | 1741.17 | 0.73 |
| | 30 | 9.97 | 9.97 | 3.62 | 0.266 | 1741.17 | |
| Filled with 3 wt% nanosilica | 0 | 13.46 | 13.46 | 3.89 | 0.266 | 1750.00 | 0.33 |
| | 30 | 11.27 | 11.28 | 3.48 | 0.266 | 1750.00 | |
| Filled with 3 wt% nanoclay | 0 | 14.06 | 14.06 | 4.52 | 0.266 | 1773.11 | 0.53 |
| | 30 | 13.65 | 13.65 | 4.09 | 0.266 | 1773.11 | |

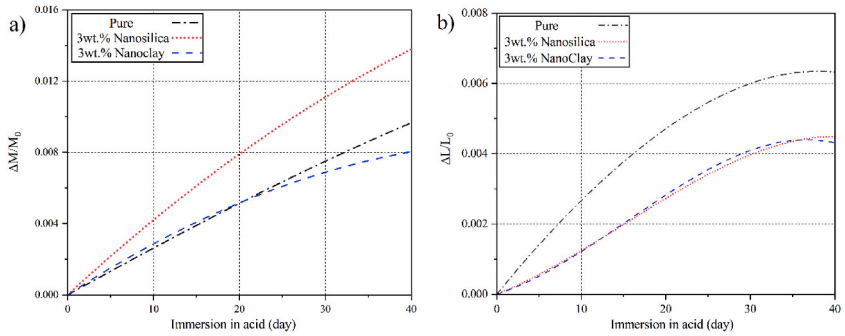


**Fig. 2.** The a) weight and b) longitudinal variation of GFRP faces during submerging in sulfuric acid.

nanocomposite, which is due to its length variation (see Fig. 2(b)).

The reinforced GFRP composites with 3 wt% of nanosilica had a lower $\rho^{acid}$, and that is for its high mass absorption (see Eq. (1)); This increase in mass may be due to the hydrophilicity of nanosilica particles, which is shown in Fig. 2(a).

The mass absorption diagram (Fig. 2(a)) demonstrates the effectiveness of incorporating clay and silica nanoparticles in saturating the faces of GFRP composites. In contrast, the pure specimens exhibited incomplete saturation and their porosity did not reach mass saturation even after one month, with no significant decrease in the rate of mass absorption.

Furthermore, by immersing the composite in an acidic medium, there is a possibility of corrosion and dissolution in acid. Dissolution can cause a decrease in the mass of specimens, and these changes were included in the results of experimental tests. According to Fig. 2, reinforced GFRP composites with 3 wt% of nanoclay had the lowest longitudinal displacement and mass absorption after one month of submerging in acid.

Experimental tensile tests were conducted to determine the mechanical properties of the manufactured composite faces. According to Table 1, the tensile modulus increased by 32.52 %, and 24.84 % by adding 3 wt% of clay, and silica nanoparticles compared to the pure composite; and after one month of immersion, reinforced GFRP faces with clay, and silica nanoparticles, and the pure composite had 2.95 %, 16.20 % and 5.99 % reduction in tensile modulus, respectively.

The shear modulus of composite faces, like the tensile elastic modulus, increases by adding the nanoparticles and decreases due to immersion in the acid. After one month of immersion, the shear modulus of filled GFRP composites with 3 wt% clay and silica nanoparticles and the pure specimens decreased by 9.38 %, 10.41 %, and 1.73 %, respectively.

Our previous research showed that the presence of hydrophobic clay nanoparticles can cause less reduction of mechanical properties of reinforced composites due to less water absorption in an acidic environment and the reduction of damages caused by corrosive environmental conditions [55].

The properties that were reported served as the material properties for the faces in the vibration analysis of the sandwich plates.

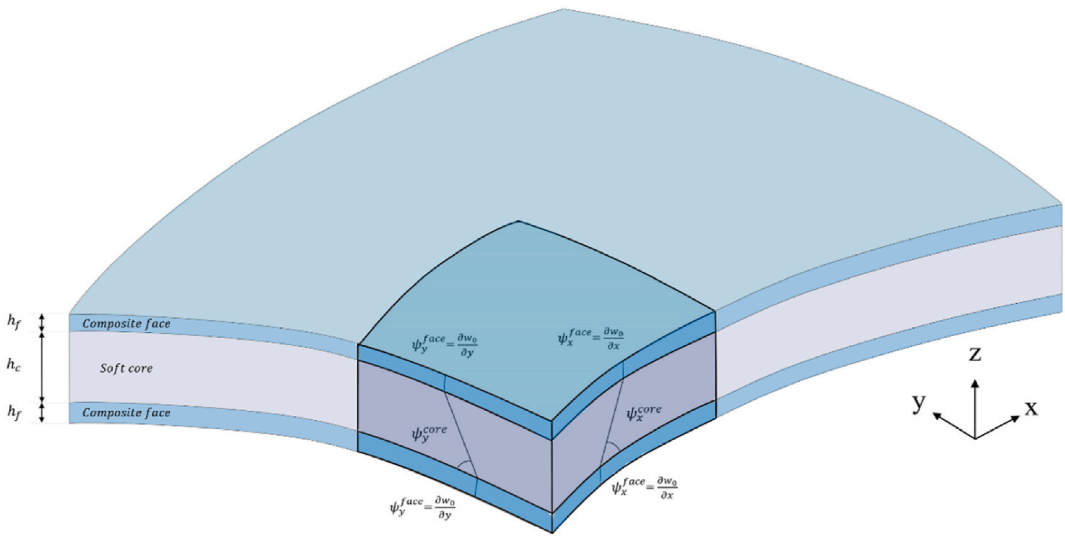


**Fig. 3.** The Sandwich plate layers, dimensions and bending deformations.

## 3. Theoretical formulation

The vibrations of sandwich with the immersion of faces in the acidic environments were studied with the LOPSDT analytical solution [73]. Fig. 3 shows a symmetrical sandwich plate with dimensions a × b × h, which consists of two composite faces with the thickness of $h_f$ and a soft core with the thickness of $h_c$ [56].

### 3.1. Governing equations

In sandwich plate vibration, it is assumed that in-plane and out-of-plane displacements of mid-plate are $u(x,y,z,t) = u_0(x,y,t)$, $v(x,y,z,t) = v_0(x,y,t)$ and $w(x,y,z,t) = w_0(x,y,t)$; The shear deformation angle of the core with respect to the mid-plane based on Fig. 3, is $\psi_1 = \psi_x^{core}$ and $\psi_2 = \psi_y^{core}$, and for composite faces, in terms of their small thickness, it is $\frac{\partial w_0}{\partial y} = \psi_y^{face}$ and $\frac{\partial w_0}{\partial x} = \psi_x^{face}$.

By the assumptions, the displacements of the sandwich in the upper and lower faces are expressed as Eq. (3) and (4).

$$\begin{aligned} u^{top}(x,y,z,t) &= u_0(x,y,t) - \frac{(2h_c+h_f)}{2}\psi_1 - \left(z - \frac{(2h_c+h_f)}{2}\right)\frac{\partial w_0}{\partial x} \\ v^{top}(x,y,z,t) &= v_0(x,y,t) - \frac{(2h_c+h_f)}{2}\psi_2 - \left(z - \frac{(2h_c+h_f)}{2}\right)\frac{\partial w_0}{\partial y} \\ w^{top}(x,y,z,t) &= w_0(x,y,t) \end{aligned} \tag{3}$$

$$\begin{aligned} u^{bottom}(x,y,z,t) &= u_0(x,y,t) + \frac{(2h_c+h_f)}{2}\psi_1 - \left(z + \frac{(2h_c+h_f)}{2}\right)\frac{\partial w_0}{\partial x} \\ v^{bottom}(x,y,z,t) &= v_0(x,y,t) + \frac{(2h_c+h_f)}{2}\psi_2 - \left(z + \frac{(2h_c+h_f)}{2}\right)\frac{\partial w_0}{\partial y} \\ w^{bottom}(x,y,z,t) &= w_0(x,y,t) \end{aligned} \tag{4}$$

Also, the displacements of the core is written as Eq. (5).

$$\begin{aligned} u^{core}(x,y,z,t) &= u_0(x,y,t) - z\left(\frac{(2h_c+h_f)}{2h_c}\psi_1 - \frac{h_f}{2h_c}\frac{\partial w_0}{\partial x}\right) \\ v^{core}(x,y,z,t) &= v_0(x,y,t) - z\left(\frac{(2h_c+h_f)}{2h_c}\psi_2 - \frac{h_f}{2h_c}\frac{\partial w_0}{\partial y}\right) \\ w^{core}(x,y,z,t) &= w_0(x,y,t) \end{aligned} \tag{5}$$

Using the linear relations of strain $\left[\varepsilon_{ij} = \frac{1}{2}(u_{i,j} + u_{j,i})\right]$, and neglecting small strains and rotations, the strain-displacement relations for faces are written as Eq. (6) and (7).

$$\begin{aligned} \varepsilon_{xx}^{top} &= \left(\frac{\partial u_0}{\partial x} - \frac{(2h_c+h_f)}{2}\frac{\partial \psi_1}{\partial x} + \frac{1}{2}\left(\frac{\partial w_0}{\partial x}\right)^2\right) + \left(z - \frac{(2h_c+h_f)}{2}\right)\left(-\frac{\partial^2 w_0}{\partial x^2}\right) \\ \varepsilon_{yy}^{top} &= \left(\frac{\partial v_0}{\partial x} - \frac{(2h_c+h_f)}{2}\frac{\partial \psi_2}{\partial y} + \frac{1}{2}\left(\frac{\partial w_0}{\partial y}\right)^2\right) + \left(z - \frac{(2h_c+h_f)}{2}\right)\left(-\frac{\partial^2 w_0}{\partial y^2}\right) \\ \varepsilon_{xy}^{top} &= \frac{1}{2}\gamma_{xy}^{top} = \frac{1}{2}\left(\left[\left(\frac{\partial u_0}{\partial y} + \frac{\partial v_0}{\partial x}\right) - \frac{(2h_c+h_f)}{2}\left(\frac{\partial \psi_1}{\partial y} + \frac{\partial \psi_2}{\partial x}\right)\right] + \left(z - \frac{(2h_c+h_f)}{2}\right)\left(-2\frac{\partial^2 w_0}{\partial x \partial y}\right)\right) \end{aligned} \tag{6}$$

And:

$$\begin{aligned} \varepsilon_{xx}^{bottom} &= \left(\frac{\partial u_0}{\partial x} + \frac{(2h_c+h_f)}{2}\frac{\partial \psi_1}{\partial x} + \frac{1}{2}\left(\frac{\partial w_0}{\partial x}\right)^2\right) + \left(z + \frac{(2h_c+h_f)}{2}\right)\left(-\frac{\partial^2 w_0}{\partial x^2}\right) \\ \varepsilon_{yy}^{bottom} &= \left(\frac{\partial v_0}{\partial x} + \frac{(2h_c+h_f)}{2}\frac{\partial \psi_2}{\partial y} + \frac{1}{2}\left(\frac{\partial w_0}{\partial y}\right)^2\right) + \left(z + \frac{(2h_c+h_f)}{2}\right)\left(-\frac{\partial^2 w_0}{\partial y^2}\right) \\ \varepsilon_{xy}^{bot} &= \frac{1}{2}\gamma_{xy}^{bottom} = \frac{1}{2}\left(\left[\left(\frac{\partial u_0}{\partial y} + \frac{\partial v_0}{\partial x}\right) + \frac{(2h_c+h_f)}{2}\left(\frac{\partial \psi_1}{\partial y} + \frac{\partial \psi_2}{\partial x}\right)\right] + \left(z + \frac{(2h_c+h_f)}{2}\right)\left(-2\frac{\partial^2 w_0}{\partial x \partial y}\right)\right) \end{aligned} \tag{7}$$

By substituting Eq. (5) in the linear strain relationship, the core strain equations can be derived as follows (Eq. (8)):

$$\varepsilon_{xx}^{core} = \left(\frac{\partial u_0}{\partial x} + \frac{1}{2}\left(\frac{\partial w_0}{\partial x}\right)^2\right) + z\left(-\frac{(2h_c + h_f)}{2h_c}\frac{\partial \psi_1}{\partial x} + \frac{h_f}{2h_c}\frac{\partial^2 w_0}{\partial x^2}\right)\left(\frac{\partial^2 w_0}{\partial x^2}\right)$$
$$\varepsilon_{yy}^{core} = \left(\frac{\partial v_0}{\partial y} + \frac{1}{2}\left(\frac{\partial w_0}{\partial y}\right)^2\right) + z\left(-\frac{(2h_c + h_f)}{2h_c}\frac{\partial \psi_2}{\partial y} + \frac{h_f}{2h_c}\frac{\partial^2 w_0}{\partial y^2}\right)\left(\frac{\partial^2 w_0}{\partial y^2}\right) \quad (8)$$
$$\varepsilon_{xy}^{core} = \frac{1}{2}\gamma_{xy}^{core} = \frac{1}{2}\left(\left(\frac{\partial u_0}{\partial y} + \frac{\partial v_0}{\partial x}\right) + z\left[-\frac{(2h_c + h_f)}{2h_c}\left(\frac{\partial \psi_1}{\partial y} + \frac{\partial \psi_2}{\partial x}\right) + \frac{h_f}{2h_c}\left(2\frac{\partial^2 w_0}{\partial x \partial y}\right)\right]\right)$$
$$\varepsilon_{xz}^{core} = \frac{1}{2}\gamma_{xz}^{core} = \frac{1}{2}\left[\frac{(2h_c + h_f)}{2h_c}\left(\frac{\partial w_0}{\partial x} - \psi_1\right)\right]$$
$$\varepsilon_{yz}^{core} = \frac{1}{2}\gamma_{yz}^{core} = \frac{1}{2}\left[\frac{(2h_c + h_f)}{2h_c}\left(\frac{\partial w_0}{\partial y} - \psi_2\right)\right]$$

The presented strains $(\varepsilon_{xx}, \varepsilon_{yy}, \gamma_{xy})$ in Eq. (8), which are related to the core of sandwich plates are linear along with the thickness, while transverse shear strains $(\gamma_{xz}, \gamma_{yz})$ remain constant via the core thickness in this theory. Stress-strain relations for core and composite surfaces will be written as Eq. (9). (In these equations, stresses from the acidic environment are assumed to be external loads.)

$$\begin{Bmatrix}\sigma_{xx}\\ \sigma_{yy}\\ \tau_{xy}\end{Bmatrix}^{(k)^{(top),(bottom),(core)}} = \begin{bmatrix}\overline{Q}_{11} & \overline{Q}_{12} & \overline{Q}_{16}\\ \overline{Q}_{12} & \overline{Q}_{22} & \overline{Q}_{26}\\ \overline{Q}_{16} & \overline{Q}_{26} & \overline{Q}_{66}\end{bmatrix}^{(k)^{(top),(bottom),(core)}} \begin{Bmatrix}\varepsilon_{xx}\\ \varepsilon_{yy}\\ \gamma_{xy}\end{Bmatrix}^{(k)^{(top),(bottom),(core)}},$$
$$\begin{Bmatrix}\tau_{yz}\\ \tau_{xz}\end{Bmatrix}^{(k)^{(core)}} = \begin{bmatrix}\overline{Q}_{44} & \overline{Q}_{45}\\ \overline{Q}_{45} & \overline{Q}_{55}\end{bmatrix}^{(k)^{(core)}} \begin{Bmatrix}\gamma_{yz}\\ \gamma_{xz}\end{Bmatrix}^{(k)^{(core)}} \quad (9)$$

Where $\overline{Q}_{ij}$ describe as Eqs. 10 and 11:

$$\begin{aligned}\overline{Q}_{11} &= Q_{11}\cos^4\theta + 2(Q_{12} + Q_{66})\sin^2\theta\cos^2\theta + Q_{22}\sin^4\theta\\ \overline{Q}_{12} &= Q_{12}(\cos^4\theta + \sin^4\theta) + (Q_{11} + Q_{22} - 4Q_{66})\sin^2\theta\cos^2\theta\\ \overline{Q}_{22} &= Q_{22}\cos^4\theta + 2(Q_{12} + Q_{66})\sin^2\theta\cos^2\theta + Q_{11}\sin^4\theta\end{aligned}$$
$$\begin{aligned}\overline{Q}_{16} &= (Q_{11} - Q_{12} - 2Q_{66})\sin\theta\cos^3\theta + (Q_{12} - Q_{22} + 2Q_{66})\cos\theta\sin^3\theta\\ \overline{Q}_{26} &= (Q_{11} - Q_{12} - 2Q_{66})\cos\theta\sin^3\theta + (Q_{12} - Q_{22} + 2Q_{66})\sin\theta\cos^3\theta\\ \overline{Q}_{66} &= (Q_{11} + Q_{22} - 2Q_{12} - 2Q_{66})\sin^2\theta\cos^2\theta + Q_{66}(\sin^4\theta + \cos^4\theta)\end{aligned} \quad (10)$$

$$\overline{Q}_{44} = Q_{44}\cos^2\theta + Q_{55}\sin^2\theta, \overline{Q}_{55} = Q_{55}\cos^2\theta + Q_{44}\sin^2\theta, \overline{Q}_{45} = (Q_{55} - Q_{44})\sin\theta\cos\theta$$

And:

$$Q_{11} = \frac{E_1}{1 - \nu_{12}\nu_{21}}, Q_{12} = \frac{\nu_{21}E_1}{1 - \nu_{12}\nu_{21}}, Q_{22} = \frac{E_2}{1 - \nu_{12}\nu_{21}}$$
$$, Q_{66} = G_{12}, Q_{44} = G_{23}, Q_{55} = G_{13} \quad (11)$$

The equations of motion are obtained by applying Hamilton's principle, which allows for the expression of the energy values of internal and external loads based on Eq. (12):

$$\int_0^T (\delta U + \delta V - \delta K)dt = 0 \quad (12)$$

The internal virtual work of the layers will be calculated as Eq. (13):

$$\delta U = \int_{\Omega_0}\int_{h_c}^{h_c+h_f}\left(\sigma_{xx}^{top}\,\delta\varepsilon_{xx}^{top} + \sigma_{yy}^{top}\,\delta\varepsilon_{yy}^{top} + 2\sigma_{xy}^{top}\,\delta\varepsilon_{xy}^{top}\right)dz\,dxdy + \int_{\Omega_0}\int_{-h_c}^{h_c}\left(\sigma_{xx}^{c}\,\delta\varepsilon_{xx}^{core} + \sigma_{yy}^{c}\,\delta\varepsilon_{yy}^{core} + 2\sigma_{xy}^{c}\,\delta\varepsilon_{xy}^{core} + 2\sigma_{xz}^{c}\,\delta\varepsilon_{xz}^{core} + 2\sigma_{yz}^{c}\,\delta\varepsilon_{yz}^{core}\right)dzdxdy$$
$$+ \int_{\Omega_0}\int_{-h_c-h_f}^{-h_c}\left(\sigma_{xx}^{bottom}\,\delta\varepsilon_{xx}^{bottom} + \sigma_{yy}^{bottom}\,\delta\varepsilon_{yy}^{bottom} + 2\sigma_{xy}^{bottom}\,\delta\varepsilon_{xy}^{bottom}\right)dz\,dxdy \quad (13)$$

By substituting the virtual strains, and taking the integral along the thickness, the internal virtual work will obtained as follows:

$$\begin{aligned}\delta U = \int_{\Omega_0} \Bigg\{ & \Bigg[ N_{xx}^{top} \left( \frac{\partial \delta u_0}{\partial x} - \frac{(2h_c + h_f)}{2} \frac{\partial \delta \psi_1}{\partial x} + \left( \frac{\partial w_0}{\partial x} \frac{\partial \delta w_0}{\partial x} \right) \right) + M_{xx}^{top} \left( - \frac{\partial^2 \delta w_0}{\partial x^2} \right) + N_{yy}^{top} \left( \frac{\partial \delta v_0}{\partial y} - \frac{(2h_c + h_f)}{2} \frac{\partial \delta \psi_2}{\partial y} + \left( \frac{\partial w_0}{\partial y} \frac{\partial \delta w_0}{\partial y} \right) \right) \\ & + M_{yy}^{top} \left( - \frac{\partial^2 \delta w_0}{\partial y^2} \right) + N_{xy}^{top} \left( \left( \frac{\partial \delta u_0}{\partial y} + \frac{\partial \delta v_0}{\partial x} \right) - \frac{(2h_c + h_f)}{2} \left( \frac{\partial \delta \psi_1}{\partial y} + \frac{\partial \delta \psi_2}{\partial x} \right) \right) + M_{xy}^{top} \left( - 2 \frac{\partial^2 \delta w_0}{\partial x \partial y} \right) \Bigg] + \Bigg[ N_{xx}^{core} \left( \frac{\partial \delta u_0}{\partial x} + \left( \frac{\partial w_0}{\partial x} \frac{\partial \delta w_0}{\partial x} \right) \right) \\ & + M_{xx}^{core} \left( - \frac{(2h_c + h_f)}{2h_c} \frac{\partial \delta \psi_1}{\partial x} + \frac{h_f}{2h_c} \frac{\partial^2 \delta w_0}{\partial x^2} \right) + N_{yy}^{core} \left( \frac{\partial \delta v_0}{\partial y} + \left( \frac{\partial w_0}{\partial y} \frac{\partial \delta w_0}{\partial y} \right) \right) + M_{yy}^{core} \left( - \frac{(2h_c + h_f)}{2h_c} \frac{\partial \delta \psi_2}{\partial y} + \frac{h_f}{2h_c} \frac{\partial^2 \delta w_0}{\partial y^2} \right) \\ & + N_{xy}^{core} \left( \left( \frac{\partial \delta u_0}{\partial y} + \frac{\partial \delta v_0}{\partial x} \right) \right) + M_{xy}^{core} \left( - \frac{(2h_c + h_f)}{2h_c} \left( \frac{\partial \delta \psi_1}{\partial y} + \frac{\partial \delta \psi_2}{\partial x} \right) + \frac{h_f}{2h_c} \left( 2 \frac{\partial^2 \delta w_0}{\partial x \partial y} \right) \right) + Q_x^{core} \left( \frac{\partial \delta w_0}{\partial x} - \delta \psi_1 \right) \\ & + Q_y^{core} \left( \frac{\partial \delta w_0}{\partial y} - \delta \psi_2 \right) \Bigg] + \Bigg[ N_{xx}^{bottom} \left( \frac{\partial \delta u_0}{\partial x} + \frac{(2h_c + h_f)}{2} \frac{\partial \delta \psi_1}{\partial x} + \left( \frac{\partial w_0}{\partial x} \frac{\partial \delta w_0}{\partial x} \right) \right) + M_{xx}^{bottom} \left( - \frac{\partial^2 \delta w_0}{\partial x^2} \right) \\ & + N_{yy}^{bottom} \left( \frac{\partial \delta v_0}{\partial x} + \frac{(2h_c + h_f)}{2} \frac{\partial \delta \psi_2}{\partial y} + \left( \frac{\partial w_0}{\partial x} \frac{\partial \delta w_0}{\partial x} \right) \right) + M_{yy}^{bottom} \left( - \frac{\partial^2 \delta w_0}{\partial y^2} \right) + N_{xy}^{bottom} \left( \left( \frac{\partial \delta u_0}{\partial y} + \frac{\partial \delta v_0}{\partial x} \right) \right. \\ & \left. + \frac{(2h_c + h_f)}{2} \left( \frac{\partial \delta \psi_1}{\partial y} + \frac{\partial \delta \psi_2}{\partial x} \right) \right) + M_{xy}^{bottom} \left( - 2 \frac{\partial^2 \delta w_0}{\partial x \partial y} \right) \Bigg] \Bigg\} \, dxdy \end{aligned} \tag{14}$$

Eq. (15) depicts the moments and forces of Eq. (14).

$$\begin{aligned} & \begin{Bmatrix} N_{xx} \\ N_{yy} \\ N_{xy} \end{Bmatrix}^{top} = \int_{h_c}^{h_c+h_f} \begin{Bmatrix} \sigma_{xx} \\ \sigma_{yy} \\ \tau_{xy} \end{Bmatrix}^{top} dz, \begin{Bmatrix} M_{xx} \\ M_{yy} \\ M_{xy} \end{Bmatrix}^{top} = \int_{h_c}^{h_c+h_f} \begin{Bmatrix} \sigma_{xx} \\ \sigma_{yy} \\ \tau_{xy} \end{Bmatrix}^{top} \left( z - \frac{2h_c + h_f}{2} \right) dz \\ & \begin{Bmatrix} N_{xx} \\ N_{yy} \\ N_{xy} \end{Bmatrix}^{bottom} = \int_{-h_c-h_f}^{-h_c} \begin{Bmatrix} \sigma_{xx} \\ \sigma_{yy} \\ \tau_{xy} \end{Bmatrix}^{bottom} dz, \begin{Bmatrix} M_{xx} \\ M_{yy} \\ M_{xy} \end{Bmatrix}^{bottom} = \int_{-h_c-h_f}^{-h_c} \begin{Bmatrix} \sigma_{xx} \\ \sigma_{yy} \\ \tau_{xy} \end{Bmatrix}^{bottom} \left( z + \frac{2h_c + h_f}{2} \right) dz \\ & \begin{Bmatrix} N_{xx} \\ N_{yy} \\ N_{xy} \end{Bmatrix}^{core} = \int_{-h_c}^{h_c} \begin{Bmatrix} \sigma_{xx} \\ \sigma_{yy} \\ \tau_{xy} \end{Bmatrix}^{core} dz, \begin{Bmatrix} M_{xx} \\ M_{yy} \\ M_{xy} \end{Bmatrix}^{core} = \int_{-h_c}^{h_c} \begin{Bmatrix} \sigma_{xx} \\ \sigma_{yy} \\ \tau_{xy} \end{Bmatrix}^{core} z \; dz, \begin{Bmatrix} Q_x \\ Q_y \end{Bmatrix}^{core} = \int_{-h_c}^{h_c} \begin{Bmatrix} \tau_{xz} \\ \tau_{yz} \end{Bmatrix}^{core} \left( \frac{2h_c + h_f}{2h_c} \right) dz \end{aligned} \tag{15}$$

The motion equations for virtual work of internal loads may be written as Eq. (16) by considering the variation in terms of virtual rotations and displacements.

$$\begin{aligned} & \delta u_0 : \frac{\partial N_{xx}}{\partial x} + \frac{\partial N_{xy}}{\partial y} \quad \delta v_0 : \frac{\partial N_{xy}}{\partial x} + \frac{\partial N_{yy}}{\partial y} \\ & \delta w_0 : \frac{\partial^2 M_{xx}}{\partial x^2} + 2 \frac{\partial^2 M_{xy}}{\partial x \partial y} + \frac{\partial^2 M_{yy}}{\partial y^2} + \left( \frac{\delta Q_x^{\,core}}{\partial x} + \frac{\delta Q_y^{\,core}}{\partial y} \right) \\ & \delta \psi_1 : \frac{2h_c + h_f}{2h_c} \left( \frac{\partial M_{xx}^{\,core}}{\partial x} + \frac{\partial M_{xy}^{\,core}}{\partial y} \right) - Q_x^{\,core} + \left( \frac{2h_c + h_f}{2} \right) \left[ \frac{\partial}{\partial x} \left( N_{xx}^{top} - N_{xx}^{bottom} \right) + \frac{\partial}{\partial y} \left( N_{xy}^{top} - N_{xy}^{bottom} \right) \right] \\ & \delta \psi_2 : \frac{2h_c + h_f}{2h_c} \left( \frac{\partial M_{xy}^{\,core}}{\partial x} + \frac{\partial M_{yy}^{\,core}}{\partial y} \right) - Q_y^{\,core} + \left( \frac{2h_c + h_f}{2} \right) \left[ \frac{\partial}{\partial x} \left( N_{xy}^{top} - N_{xy}^{bottom} \right) + \frac{\partial}{\partial y} \left( N_{yy}^{top} - N_{yy}^{bottom} \right) \right] \end{aligned} \tag{16}$$

where forces are described as Eq. (17).

$$\begin{Bmatrix} N_{xx} \\ N_{yy} \\ N_{xy} \end{Bmatrix} = \begin{Bmatrix} N_{xx}^{top} + N_{xx}^{core} + N_{xx}^{bottom} \\ N_{yy}^{top} + N_{yy}^{core} + N_{yy}^{bottom} \\ N_{xy}^{top} + N_{xy}^{core} + N_{xy}^{bottom} \end{Bmatrix} \begin{Bmatrix} M_{xx} \\ M_{yy} \\ M_{xy} \end{Bmatrix} = \begin{Bmatrix} M_{xx}^{top} - \frac{h_f}{2h_c} M_{xx}^{core} + M_{xx}^{bottom} \\ M_{yy}^{top} - \frac{h_f}{2h_c} M_{yy}^{core} + M_{yy}^{bottom} \\ M_{xy}^{top} - \frac{h_f}{2h_c} M_{xy}^{core} + M_{xy}^{bottom} \end{Bmatrix} \tag{17}$$

The virtual work of the kinetic energy of the sandwich plate will also be calculated as follows:

$$\begin{aligned}\delta K &= \int \left(\delta K^{top} + \delta K^{core} + \delta K^{bottom}\right) dV \\ &= = \int_{\Omega_0} \left\{ \int_{h_c}^{h_c+h_f} \rho^{top} \left(\dot{u}^{top}\, \delta\dot{u}^{top} + \dot{v}^{top}\, \delta\dot{v}^{top} + \dot{w}^{top}\, \delta\dot{w}^{top}\right) dz + \int_{-h_c}^{h_c} \rho^{core} \left(\dot{u}^{core}\, \delta\dot{u}^{core} + \dot{v}^{core}\, \delta\dot{v}^{core} + \dot{w}^{core}\, \delta\dot{w}^{core}\right) dz \right. \\ &\left. + \int_{-h_c-h_f}^{-h_c} \rho^{bottom} \left(\dot{u}^{bottom}\, \delta\dot{u}^{bottom} + \dot{v}^{bottom}\, \delta\dot{v}^{bottom} + \dot{w}^{bottom}\, \delta\dot{w}^{bottom}\right) dz \right\} dxdy\end{aligned} \tag{18}$$

By substituting the virtual strain into Eq. (18), and taking the integral along the thickness:

$$\begin{aligned}\delta K = \int_{\Omega_0} \Big[ &- I_0^{face}(\dot{u}_0\delta\dot{u}_0 + \dot{v}_0\delta\dot{v}_0 + \dot{w}_0\delta\dot{w}_0) + I_1^{face}(\dot{\psi}_1\delta\dot{\psi}_1 + \dot{\psi}_2\delta\dot{\psi}_2) + I_3^{face}\left(\frac{\partial\dot{w}_0}{\partial x}\frac{\partial\delta\dot{w}_0}{\partial x} + \frac{\partial\dot{w}_0}{\partial y}\frac{\partial\delta\dot{w}_0}{\partial y}\right) - I_0^{core}(\dot{u}_0\delta\dot{u}_0 + \dot{v}_0\delta\dot{v}_0 + \dot{w}_0\delta\dot{w}_0) \\ &+ I_1^{core}(\dot{\psi}_1\delta\dot{\psi}_1 + \dot{\psi}_2\delta\dot{\psi}_2) + I_3^{core}\left(\frac{\partial\dot{w}_0}{\partial x}\frac{\partial\delta\dot{w}_0}{\partial x} + \frac{\partial\dot{w}_0}{\partial y}\frac{\partial\delta\dot{w}_0}{\partial y}\right) - I_2^{core}\left(\dot{\psi}_1\frac{\partial\delta\dot{w}_0}{\partial x} + \dot{\psi}_2\frac{\partial\delta\dot{w}_0}{\partial y} + \frac{\partial\dot{w}_0}{\partial x}\delta\dot{\psi}_1 + \frac{\partial\dot{w}_0}{\partial y}\delta\dot{\psi}_2\right)\Big] dxdy\end{aligned} \tag{19}$$

where Eq. (20) describes the $I_i^{(k)}$ in Eq. (19).

$$I_0^{face} = 2\int_{h_c}^{h_c+h_f} \rho^{face}\, dz, I_1^{face} = 2\int_{h_c}^{h_c+h_f} \rho^{face}\left(\frac{2h_c+h_f}{2h_c}\right)^2 dz, I_3^{face} = 2\int_{h_c}^{h_c+h_f} \rho^{face}\left(z - \frac{2h_c+h_f}{2h_c}\right)^2 dz,$$

$$I_0^{core} = \int_{-h_c}^{h_c} \rho^{core}\, dz, I_1^{core} = \int_{-h_c}^{h_c} \rho^{core}\left(\frac{2h_c+h_f}{2h_c}\right)^2 z^2\, dz, I_2^{core} = \int_{-h_c}^{h_c} \rho^{core}\left(\frac{2h_c+h_f}{2h_c}\right)\frac{h_f}{2h_c}\, z^2\, dz, I_3^{core} = \int_{-h_c}^{h_c} \rho^{core}\left(\frac{h_f}{2h_c}\right)^2 z^2\, dz \tag{20}$$

By solving the equations with the variational method, virtual work equations of the kinetic energy will be written as follows:

$$\delta u_0 : I_0\frac{\partial^2 u_0}{\partial t^2}, \delta v_0 : I_0\frac{\partial^2 v_0}{\partial t^2}, \delta w_0 : I_0\frac{\partial^2 w_0}{\partial t^2} + I_2\left(\frac{\partial^3\psi_1}{\partial x\partial t^2} + \frac{\partial^3\psi_2}{\partial y\partial t^2}\right) - I_3\left(\frac{\partial^4 w_0}{\partial x^2\partial t^2} + \frac{\partial^4 w_0}{\partial y^2\partial t^2}\right),$$

$$\delta\psi_1 : -I_1\frac{\partial^2\psi_1}{\partial t^2} + I_2\frac{\partial^3 w_0}{\partial x\partial t^2}, \delta\psi_2 : -I_1\frac{\partial^2\psi_2}{\partial t^2} + I_2\frac{\partial^3 w_0}{\partial y\partial t^2} \tag{21}$$

where moments of inertia are defined as Eq. (22).

$$I_0 = I_0^{face} + I_0^{core}, I_1 = I_1^{face} + I_1^{core}, I_2 = I_2^{core}, I_3 = I_3^{face} + I_3^{core} \tag{22}$$

The virtual work of external forces is calculated as follows: (It is assumed that only the faces are in contact with sulfuric acid, and by using a proper adhesive, the core will not be in contact with the corrosive environment; therefore, the environmental load is applied only to faces.)

$$\delta V = -\int q\, .\delta u_i\, dv = \left(N_x^{(acid)}\frac{\partial^2 w_0}{\partial x^2} + N_y^{(acid)}\frac{\partial^2 w_0}{\partial y^2}\right)\delta w_0 \tag{23}$$

In Eq. (23), the force values due to the acidic environment will be obtained by Eqs. 24 and 25.

$$N_x^{(acid)} = N_x^{(acid)^{top}} + N_x^{(acid)^{bottom}}, N_y^{(acid)} = N_y^{(acid)^{top}} + N_y^{(acid)^{bottom}} \tag{24}$$

Where:

$$\begin{Bmatrix} N_x^{(acid)} \\ N_y^{(acid)} \\ N_{xy}^{(acid)} \end{Bmatrix}^{(k)^{(top),(bottom)}} = \sum_{k=1}^{N} \int_{z_k}^{z_{k+1}} \begin{bmatrix} \overline{Q}_{11} & \overline{Q}_{12} & \overline{Q}_{16} \\ \overline{Q}_{12} & \overline{Q}_{22} & \overline{Q}_{26} \\ \overline{Q}_{16} & \overline{Q}_{26} & \overline{Q}_{66} \end{bmatrix}^{(k)^{(top),(bottom)}} \begin{Bmatrix} \beta_{xx}^{\ acid} \\ \beta_{yy}^{\ acid} \\ (2\beta_{xy}^{\ acid} = 0) \end{Bmatrix}^{(k)^{(top),(bottom)}} \left(\frac{\Delta m}{m_0}\right)^{(k)^{(top),(bottom)}} dz \tag{25}$$

The equations of motion for the sandwich plate under the environmental load caused by immersion in sulfuric acid are calculated using equations (16), (21) and (23):

$$\delta u_0 : \frac{\partial N_{xx}}{\partial x} + \frac{\partial N_{xy}}{\partial y} = I_0\frac{\partial^2 u_0}{\partial t^2} \quad \delta v_0 : \frac{\partial N_{xy}}{\partial x} + \frac{\partial N_{yy}}{\partial y} = I_0\frac{\partial^2 v_0}{\partial t^2} \tag{26}$$

$$\delta w_0 : \frac{\partial^2 M_{xx}}{\partial x^2} + 2\frac{\partial^2 M_{xy}}{\partial x\partial y} + \frac{\partial^2 M_{yy}}{\partial y^2} + \mathbb{N}^{acid}(w_0) + \left(\frac{\delta Q_x^{\ core}}{\partial x} + \frac{\delta Q_y^{\ core}}{\partial y}\right) = I_0\frac{\partial^2 w_0}{\partial t^2} + I_2\left(\frac{\partial^3\psi_1}{\partial x\partial t^2} + \frac{\partial^3\psi_2}{\partial y\partial t^2}\right) - I_3\left(\frac{\partial^4 w_0}{\partial x^2\partial t^2} + \frac{\partial^4 w_0}{\partial y^2\partial t^2}\right)$$

$$\delta\psi_1 : \frac{2h_c+h_f}{2h_c}\left(\frac{\partial M_{xx}^{\ core}}{\partial x} + \frac{\partial M_{xy}^{\ core}}{\partial y}\right) - Q_x^{\ core} + \left(\frac{2h_c+h_f}{2}\right)\left[\frac{\partial}{\partial x}\left(N_{xx}^{top} - N_{xx}^{bottom}\right) + \frac{\partial}{\partial y}\left(N_{xy}^{top} - N_{xy}^{bottom}\right)\right] = -I_1\frac{\partial^2\psi_1}{\partial t^2} + I_2\frac{\partial^3 w_0}{\partial x\partial t^2}$$

$$\delta\psi_2 : \frac{2h_c+h_f}{2h_c}\left(\frac{\partial {M_{xy}}^{core}}{\partial x}+\frac{\partial {M_{yy}}^{core}}{\partial y}\right)-{Q_y}^{core}+\left(\frac{2h_c+h_f}{2}\right)\left[\frac{\partial}{\partial x}\left(N_{xy}^{top}-N_{xy}^{bottom}\right)+\frac{\partial}{\partial y}\left(N_{yy}^{top}-N_{yy}^{bottom}\right)\right]=-I_1\frac{\partial^2\psi_2}{\partial t^2}+I_2\frac{\partial^3 w_0}{\partial y\partial t^2}$$

The equations of motion (26) can be expressed with the displacement parameters as Eq. (27) using Eq. 9 and 15.

$$\delta u_0 : g_{11}^{(4)}\left(\frac{\partial}{\partial x}\left(\frac{\partial u_0}{\partial x}+\frac{1}{2}\left(\frac{\partial w_0}{\partial x}\right)^2\right)\right)+g_{12}^{(4)}\left(\frac{\partial}{\partial x}\left(\frac{\partial v_0}{\partial y}+\frac{1}{2}\left(\frac{\partial w_0}{\partial y}\right)^2\right)\right)+g_{66}^{(4)}\left(\frac{\partial}{\partial y}\left(\frac{\partial u_0}{\partial y}+\frac{\partial v_0}{\partial x}\right)\right)=I_0\frac{\partial^2 u_0}{\partial t^2} \tag{27}$$

$$\delta v_0 : g_{22}^{(4)}\left(\frac{\partial}{\partial y}\left(\frac{\partial v_0}{\partial y}+\frac{1}{2}\left(\frac{\partial w_0}{\partial y}\right)^2\right)\right)+g_{12}^{(4)}\left(\frac{\partial}{\partial y}\left(\frac{\partial u_0}{\partial x}+\frac{1}{2}\left(\frac{\partial w_0}{\partial x}\right)^2\right)\right)+g_{66}^{(4)}\left(\frac{\partial}{\partial x}\left(\frac{\partial u_0}{\partial y}+\frac{\partial v_0}{\partial x}\right)\right)=I_0\frac{\partial^2 v_0}{\partial t^2}$$

$$\delta w_0 : g_{11}^{(3)}\frac{\partial^4 w_0}{\partial x^4}+\left(2g_{12}^{(3)}+4g_{66}^{(3)}\right)\frac{\partial^4 w_0}{\partial y^2\partial x^2}+g_{22}^{(3)}\frac{\partial^4 w_0}{\partial y^4}-g_{11}^{(2)}\frac{\partial^3\psi_1}{\partial x^3}-g_{22}^{(2)}\frac{\partial^3\psi_2}{\partial y^3}-\left(g_{12}^{(2)}+2g_{66}^{(2)}\right)\left(\frac{\partial^3\psi_1}{\partial x\partial y^2}+\frac{\partial^3\psi_2}{\partial y\partial x^2}\right)+S_{cxz}\left(\frac{\partial\psi_1}{\partial x}-\frac{\partial^2 w_0}{\partial x^2}\right)$$
$$+S_{cyz}\left(\frac{\partial\psi_2}{\partial y}-\frac{\partial^2 w_0}{\partial y^2}\right)+\left(N_x^{(acid)}\frac{\partial^2 w_0}{\partial x^2}+N_y^{(acid)}\frac{\partial^2 w_0}{\partial y^2}\right)=-I_0\frac{\partial^2 w_0}{\partial t^2}-I_2\left(\frac{\partial^3\psi_1}{\partial x\partial t^2}+\frac{\partial^3\psi_2}{\partial y\partial t^2}\right)+I_3\left(\frac{\partial^4 w_0}{\partial x^2\partial t^2}+\frac{\partial^4 w_0}{\partial y^2\partial t^2}\right)$$

$$\delta\psi_1 : g_{11}^{(2)}\frac{\partial^3 w_0}{\partial x^3}+\left(g_{12}^{(2)}+2g_{66}^{(2)}\right)\frac{\partial^3 w_0}{\partial y^2\partial x}-\left(g_{12}^{(1)}+2g_{66}^{(1)}\right)\frac{\partial^2\psi_2}{\partial y\partial x}-g_{11}^{(1)}\frac{\partial^2\psi_1}{\partial x^2}-g_{66}^{(1)}\frac{\partial^2\psi_1}{\partial y^2}+S_{cxz}\left(\psi_1-\frac{\partial w_0}{\partial x}\right)=-I_1\frac{\partial^2\psi_1}{\partial t^2}+I_2\frac{\partial^3 w_0}{\partial x\partial t^2}$$

$$\delta\psi_2 : g_{22}^{(2)}\frac{\partial^3 w_0}{\partial y^3}+\left(g_{12}^{(2)}+2g_{66}^{(2)}\right)\frac{\partial^3 w_0}{\partial x^2\partial y}-\left(g_{12}^{(1)}+2g_{66}^{(1)}\right)\frac{\partial^2\psi_1}{\partial y\partial x}-g_{22}^{(1)}\frac{\partial^2\psi_2}{\partial y^2}-g_{66}^{(1)}\frac{\partial^2\psi_2}{\partial x^2}+S_{cyz}\left(\psi_2-\frac{\partial w_0}{\partial y}\right)=-I_1\frac{\partial^2\psi_2}{\partial t^2}+I_2\frac{\partial^3 w_0}{\partial y\partial t^2}$$

Which the constant values of $g_{ij}^{(k)}$ are calculated by Eqs. 28 and 29.

$$g_{11}^{(2)}=D_{11}^{core}\left(\frac{h_f+2h_c}{2h_c}\right)\left(\frac{h_f}{2h_c}\right)\ g_{11}^{(1)}=2A_{11}^{face}\left(\frac{h_f+2h_c}{2}\right)^2+D_{11}^{core}\left(\frac{h_f+2h_c}{2h_c}\right)^2 \tag{28}$$

$$g_{12}^{(2)}=D_{12}^{core}\left(\frac{h_f+2h_c}{2h_c}\right)\left(\frac{h_f}{2h_c}\right)\ g_{12}^{(1)}=2A_{12}^{face}\left(\frac{h_f+2h_c}{2}\right)^2+D_{12}^{core}\left(\frac{h_f+2h_c}{2h_c}\right)^2$$

$$g_{22}^{(2)}=D_{22}^{core}\left(\frac{h_f+2h_c}{2h_c}\right)\left(\frac{h_f}{2h_c}\right)\ g_{22}^{(1)}=2A_{22}^{face}\left(\frac{h_f+2h_c}{2}\right)^2+D_{22}^{core}\left(\frac{h_f+2h_c}{2h_c}\right)^2$$

$$g_{66}^{(2)}=D_{66}^{core}\left(\frac{h_f+2h_c}{2h_c}\right)\left(\frac{h_f}{2h_c}\right)\ g_{66}^{(1)}=2A_{66}^{face}\left(\frac{h_f+2h_c}{2}\right)^2+D_{66}^{core}\left(\frac{h_f+2h_c}{2h_c}\right)^2$$

$$g_{11}^{(4)}=2A_{11}^{face}+A_{11}^{core}\ g_{11}^{(3)}=2D_{11}^{face}+D_{11}^{core}\left(\frac{h_f}{2h_c}\right)^2$$

$$g_{12}^{(4)}=2A_{12}^{face}+A_{12}^{core}\ g_{12}^{(3)}=2D_{12}^{face}+D_{12}^{core}\left(\frac{h_f}{2h_c}\right)^2$$

$$g_{22}^{(4)}=2A_{22}^{face}+A_{22}^{core}\left(3\right)=2D_{22}^{face}+D_{22}^{core}\left(\frac{h_f}{2h_c}\right)^2$$

$$g_{66}^{(4)}=2A_{66}^{face}+A_{66}^{core}\ g_{66}^{(3)}=2D_{66}^{face}+D_{66}^{core}\left(\frac{h_f}{2h_c}\right)^2$$

$$S_{cxz}=A_{55}{}^{core}\left(\frac{2h_c+h_f}{2h_c}\right)^2\ S_{cyz}=A_{44}{}^{core}\left(\frac{2h_c+h_f}{2h_c}\right)^2$$

$$A_{ij}^{(face)}=\int_{h_c}^{h_c+h_f}\overline{Q}_{ij}{}^{(face)(top)}\ dz=\int_{-h_c-h_f}^{-h_c}\overline{Q}_{ij}^{(face)(bottom)}\ dz, \tag{29}$$

$$D_{ij}^{(face)}=\int_{h_c}^{h_c+h_f}\overline{Q}_{ij}{}^{(face)(top)}\left(z-\frac{(2h_c+h_f)}{2}\right)^2\ dz=\int_{-h_c-h_f}^{-h_c}\overline{Q}_{ij}^{(face)(bottom)}\left(z+\frac{(2h_c+h_f)}{2}\right)^2\ dz,$$

$$A_{ij}^{(core)} = \int_{-h_c}^{h_c} \overline{Q}_{ij}^{(core)} \quad dz, D_{ij}^{(core)} = \int_{-h_c}^{h_c} \overline{Q}_{ij}^{(core)} z^2 \ dz$$

### 3.2. Vibration analysis

The out-plane vibrations of sandwich plate are analyzed. The sandwich equations of motion extracted in the previous section included five motion equations based on the displacement quantities for $(u_0, v_0, w_0, \psi_1, \psi_2)$, and in terms of uncoupling of the first two equations, they can be eliminated. To address the SSSS boundary condition of the displacement field for variables $(w_0, \psi_1, \psi_2)$, an expansion using trigonometric series, including double series, is employed. This expansion involves utilizing undefined variables and is used to solve the boundary condition as expressed in Eq. (30).

$$\begin{aligned} w_0(x,y,t) &= \sum_{n=1}^{\infty}\sum_{m=1}^{\infty} W_{mn}(t) \times sin\ \alpha t\ sin\ \beta y \\ \psi_1(x,y,t) &= \sum_{n=1}^{\infty}\sum_{m=1}^{\infty} X_{mn}(t) \times cos\ \alpha t\ sin\ \beta y \\ \psi_2(x,y,t) &= \sum_{n=1}^{\infty}\sum_{m=1}^{\infty} Y_{mn}(t) \times sin\ \alpha t\ cos\ \beta y \end{aligned} \tag{30}$$

Within Eq. (30), the variables $\alpha$ and β are defined as $\alpha = \frac{m\pi}{a}$ and $\beta = \frac{n\pi}{b}$, where m and n correspond to the number of semi-waves present in the x and y directions, respectively.

The outcome will be as follows by replacing Eq. (30) in the equations of motion:

$$\begin{bmatrix} C_{11}+f_1 & C_{12} & C_{13} \\ C_{12} & C_{22} & C_{23} \\ C_{13} & C_{23} & C_{33} \end{bmatrix} \begin{Bmatrix} W_{mn} \\ X_{mn} \\ Y_{mn} \end{Bmatrix} - \omega^2 \begin{bmatrix} M_{11} & M_{12} & M_{13} \\ M_{12} & M_{22} & M_{23} \\ M_{13} & M_{23} & M_{33} \end{bmatrix} \begin{Bmatrix} W_{mn} \\ X_{mn} \\ Y_{mn} \end{Bmatrix} = 0 \tag{31}$$

The coefficients of matrix, $C_{ij}$ and $M_{ij}$, will be obtained as Eq. (32).

$$\begin{aligned} C_{11} &= g_{11}^{(3)}(bm\pi)^4 + g_{22}^{(3)}(an\pi)^4 + \left(2g_{12}^{(3)} + 4g_{66}^{(3)}\right)(abmn\pi)^2 + S_{cxz}(am\pi)^2(b)^4 + S_{cxz}(bn\pi)^2(a)^4 \\ C_{12} &= -g_{11}^{(2)}(m\pi b)^3\ ab - \left(g_{12}^{(2)} + 2g_{66}^{(2)}\right)\left(a^3b^2mn^2\pi^2\right) - S_{cxz}\left(a^3b^4m\pi\right) \\ C_{13} &= -g_{22}^{(2)}(n\pi a)^3\ ab - \left(g_{12}^{(2)} + 2g_{66}^{(2)}\right)\left(b^3a^2nm^2\pi^2\right) - S_{cyz}\left(b^3a^4n\pi\right) \end{aligned}$$

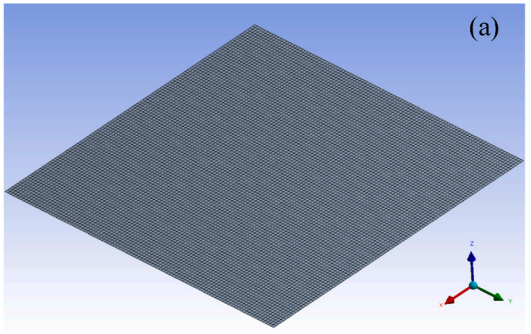


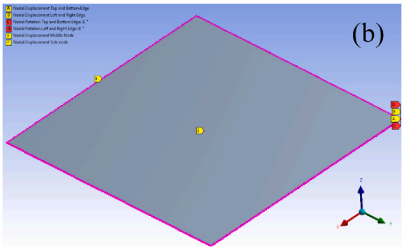


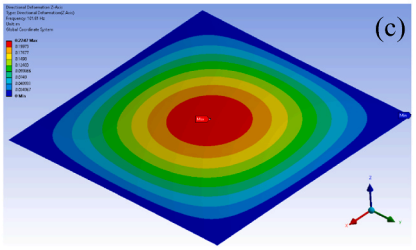


**Fig. 4.** FE model of Ansys software for a) mesh modeling, b) boundary conditions, and c) vibration analysis for mode (1,1).

$$C_{22} = g_{11}^{(1)}(am\pi)^2 b^4 + g_{66}^{(1)}(bn\pi)^2 a^4 + S_{cxz}(ab)^4$$
$$C_{23} = \left(g_{12}^{(1)} + g_{66}^{(1)}\right)(mn\pi^2)(ab)^3$$
$$C_{33} = g_{22}^{(1)}(bn\pi)^2 a^4 + g_{66}^{(1)}(am\pi)^2 b^4 + S_{cyz}(ab)^4$$

$$M_{11} = I_0\,(ab)^4 + I_3\left(\left(ab^2 m\pi\right)^2 + \left(ba^2 n\pi\right)^2\right), M_{12} = -I_2\left(a^3 b^4 m\pi\right)$$
$$M_{13} = -I_2\left(a^4 b^3 m\pi\right), M_{22} = -I_1(ab)^4, M_{23} = 0, M_{33} = -I_1(ab)^4 f_1 = N_x^{(m)}\left(ab^2 m\pi\right)^2 + N_y^{(m)}\left(ba^2 n\pi\right)^2 \quad (32)$$

Eq. (31), creates an eigenvalue matrix that the natural frequency and the frequency under environmental load will be calculated based on the following equation.

$$det\ \left[[C] - \omega^2\,[M]\right] = 0 \quad (33)$$

In Eq. (33), the positive and real values will be the correct answer of $\omega^2$ which is shown as $\omega_{mn}$ for each mode shape [74].

### 3.3. Finite element evaluation in validating natural frequency

The theoretical solution will be validated by the Ansys numerical solution. The sandwich plate is modeled as a surface, and with SHELL181 elements according to Fig. 4(a); and the definition of boundary condition, and contour results of the free vibration of sandwich was illustrated in Fig. 4 (b, c).

Mesh sensitivity analysis for the natural frequency of sandwich with incorporated faces by 3 wt% of nanoclay was checked in different modes before immersion in sulfuric acid; And as the results show in Table 2, increasing the number of elements in the sandwich is effective on results. The frequency converges in the 100 × 100 number of elements.

Vibration analysis is performed on the sandwich structure with the dimensions of 1000 *mm* × 1000 *mm* and thickness of 55 *mm*. In this analysis, the thickness of core is 50 *mm*, and the thickness of each face is 2.5 *mm*. The isotropic core of the sandwich structure exhibits the following mechanical properties: $E_1 = 3\ Gpa, \nu_{12} = 0.4, \rho = 1400\frac{Kg}{m^3}$ [75].

In Table 3, the analytical solution and ANSYS finite element are compared, and the results showed good accuracy. Therefore, the analytical solution can be used to calculate the natural frequency and frequency under pre-stress due to immersion in acid.

## 4. Results and discussion

The accuracy of the results and good agreement between the analytical solution using LOPSDT and the ANSYS solution were demonstrated in the previous section. This section presents the sandwich's natural frequency and its frequency under environmental stress and investigates the sandwich plate's vibration frequency as a result of the addition of 3 wt% of nanosilica and nanoclay to the GFRP composite faces in an acidic medium.

### 4.1. Natural frequency of sandwich plate in the acid immersion

Based on Fig. 5(a), by adding nanoparticles, the natural frequency of sandwich plate is increased before immersion in acid; This increase can be due to the strengthening of mechanical properties by adding clay and silica nanoparticles to the epoxy glass composites faces.

Based on the findings provided in Table 1, the inclusion of 3 wt% of nanoclay demonstrates a greater improvement in the mechanical properties of the GFRP composite face compared to the addition of 3 wt% of nanosilica. Consequently, the natural frequency of the sandwich structure with a GFRP composite face reinforced by 3 wt% of nanoclay surpasses that of the sandwich structure with a face containing 3 wt% of nanosilica.

Fig. 5(a) shows that adding 3 wt% of nanoclay to the pure composite faces in the sandwich caused a 6.81 % increase in the natural frequency of the first mode; Also, there is an increase of 4 %–6 % in other modes.

The variation in natural frequency of the sandwich plates following one month of acid immersion is depicted in Fig. 5(b). Through a

**Table 2**
Mesh sensitivity analysis for natural frequency (Hz) of sandwich plate with reinforced composite face by 3 wt% of nanoclay before immersion in acid for FE model.

| Element NO. | **Modes** $(m,n)$ | | | | | |
|---|---|---|---|---|---|---|
| | $(1,1)$ | $(1,2)$ | $(2,2)$ | $(2,3)$ | $(1,4)$ | $(3,3)$ |
| 10 × 10 | 102.90 | 278.83 | 403.79 | 660.37 | 932.85 | 884.60 |
| 20 × 20 | 102.07 | 263.65 | 391.57 | 621.32 | 822.13 | 829.66 |
| 40 × 40 | 101.86 | 258.26 | 388.60 | 612.82 | 796.06 | 816.62 |
| 50 × 50 | 101.84 | 257.35 | 388.25 | 611.71 | 792.78 | 815.07 |
| 100 × 100 | 101.81 | 255.60 | 387.78 | 610.17 | 788.03 | 813.02 |
| 200 × 200 | 101.80 | 254.84 | 387.66 | 609.73 | 786.60 | 812.50 |

**Table 3**
Validation of the frequency of analytical solution with Ansys numerical solution.

| Fabricated GFRP composites | Solutions Method | Modes $(m,n)$ | | | | | |
|---|---|---|---|---|---|---|---|
| | | (1,1) | (1,2) | (2,2) | (2,3) | (1,4) | (3,3) |
| Sandwich Plate with pure composite face before immersion | Ansys (Hz) | 95.34 | 239.59 | 364.79 | 575.26 | 741.76 | 769.28 |
| | Analytical (Hz) | 95.40 | 234.21 | 365.57 | 575.88 | 739.37 | 772.53 |
| | Error (%) | 0.06 | 2.29 | 0.21 | 0.11 | 0.32 | 0.42 |
| Sandwich Plate with pure composite face after one month of immersion | Ansys (Hz) | 94.27 | 236.73 | 360.92 | 569.15 | 732.75 | 761.80 |
| | Analytical (Hz) | 94.33 | 231.34 | 361.73 | 569.80 | 730.31 | 765.13 |
| | Error (%) | 0.06 | 2.33 | 0.22 | 0.12 | 0.36 | 0.44 |
| Sandwich Plate with incorporation of 3 wt% nanosilica into the face before immersion | Ansys (Hz) | 99.79 | 251.53 | 380.70 | 600.38 | 779.37 | 799.79 |
| | Analytical (Hz) | 99.85 | 246.22 | 381.43 | 600.90 | 777.22 | 802.76 |
| | Error (%) | 0.05 | 2.16 | 0.19 | 0.09 | 0.28 | 0.37 |
| Sandwich Plate with incorporation of 3 wt% nanosilica into the face after one month of immersion | Ansys (Hz) | 95.85 | 241.57 | 366.63 | 578.80 | 749.93 | 772.89 |
| | Analytical (Hz) | 95.91 | 236.24 | 367.38 | 579.34 | 747.63 | 775.96 |
| | Error (%) | 0.06 | 2.26 | 0.20 | 0.09 | 0.31 | 0.40 |
| Sandwich Plate with incorporation of 3 wt% nanoclay into the face before immersion | Ansys (Hz) | 101.81 | 255.60 | 387.78 | 610.17 | 788.03 | 813.02 |
| | Analytical (Hz) | 101.86 | 250.24 | 388.54 | 610.78 | 785.88 | 816.14 |
| | Error (%) | 0.05 | 2.14 | 0.20 | 0.10 | 0.27 | 0.38 |
| Sandwich Plate with incorporation of 3 wt% nanoclay into the face after one month immersion | Ansys (Hz) | 100.39 | 252.70 | 382.79 | 603.22 | 781.71 | 803.64 |
| | Analytical (Hz) | 100.45 | 247.38 | 383.53 | 603.77 | 779.55 | 806.66 |
| | Error (%) | 0.06 | 2.15 | 0.19 | 0.09 | 0.28 | 0.37 |

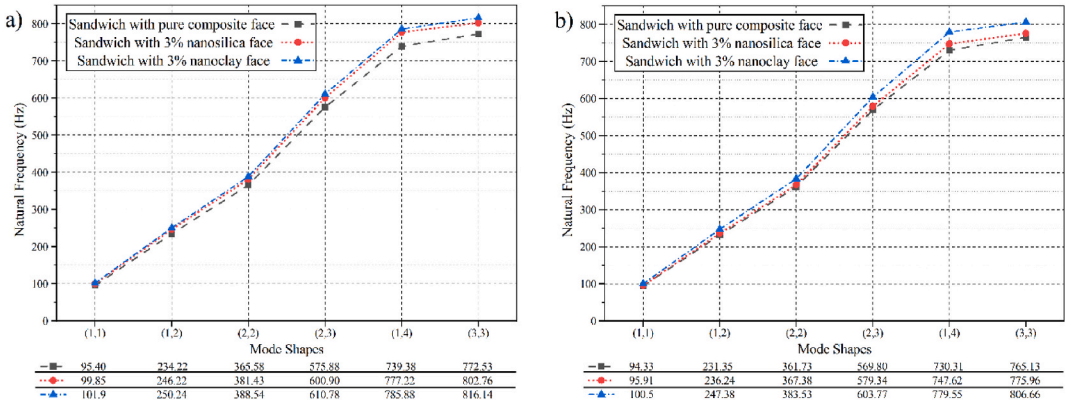


**Fig. 5.** The comparisons of natural frequency of sandwich plates in a) 0 day, and b) 30 day of immerision in acid.

comparison of Fig. 5(a) and (b), it can be observed that the natural frequencies of the sandwich plates with faces reinforced by 3 wt% of nanosilica tend towards the natural frequency of the sandwich plates with pure faces after the month-long immersion in sulfuric acid. This decline in natural frequency can be attributed to the water absorption by the silica particles within the composite faces, leading to a degradation in their mechanical properties in the acidic environment. Conversely, the sandwich plates with GFRP faces reinforced by 3 wt% of nanoclay exhibit a lesser reduction in natural frequency and maintain a higher natural frequency even after the one-month immersion period.

Upon analyzing the sandwich plate following a one-month immersion period, it was observed that the natural frequency of the sandwich plate with the pure composite face and the one incorporating 3 wt% of nanoclay experienced a decrease of approximately 1 %. In contrast, the sandwich plate with the face containing 3 wt% of nanosilica exhibited a higher reduction of over 3 % in its natural frequency.

### *4.2. Frequency of sandwich plate under pre-stress of acidic environment*

In the experimental tests, it was observed that immersion in the sulfuric acid causes GFRP composite to swell in longitudinal directions. In the analysis of forced vibrations, because of the swelling of the sandwich, fixed boundaries in the simply supported plate, cause normal force due to the pre-stress of acidic environments. Using the $\beta^{acid}$ and the amount of mass absorption of the faces (see Fig. 2(a)), the normal force on the sandwich will be obtained from Eq. (2) and Eq. (26). By obtained force, the vibration frequency of sandwich plate under the pre-stress of the acidic environment can be calculated.

In this solution, the variation of mechanical properties in one month of submerging is assumed to be linear, and $\beta^{acid}$ is constant; In this case, the only factor that causes the results to be non-linear is the absorption of the mass in the faces, which is shown in Fig. 2(a).

Fig. 6 is presented the results of frequency for 6 mode shapes. Fig. 6, shows immersion in acid, and environment pre-stress on the

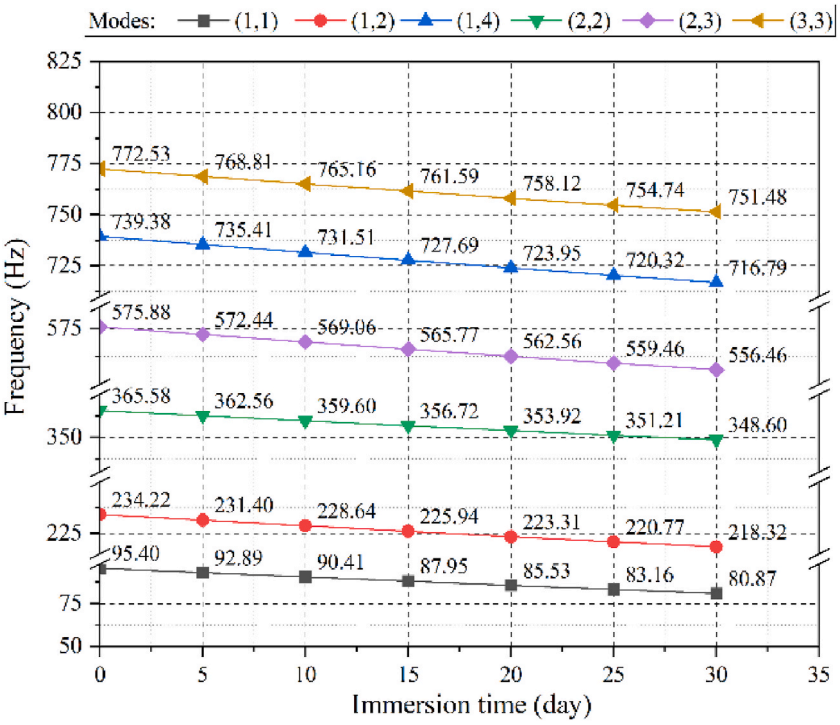


**Fig. 6.** Frequency of forced vibration of sandwich with pure face in one month of immersion.

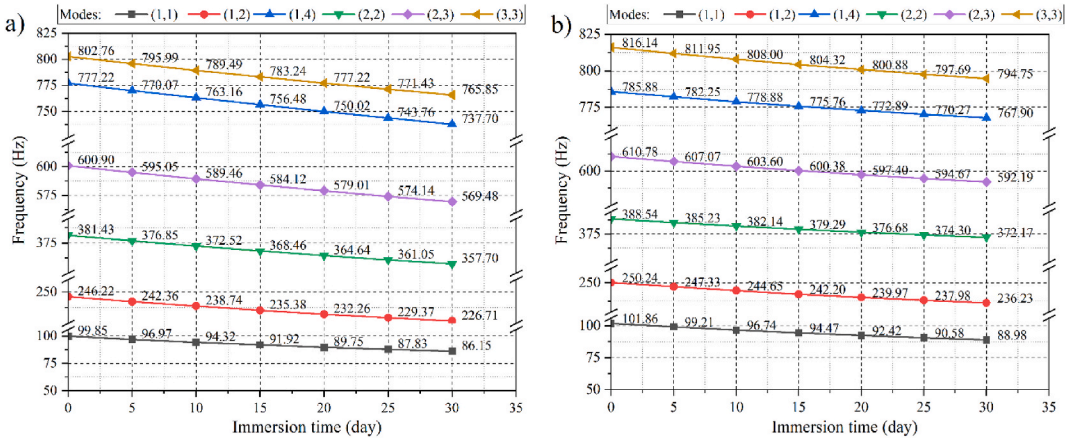


**Fig. 7.** Frequency of forced vibration of sandwich with a) 3 wt% of nanosilica and b) 3 wt% of nanoclay faces in one month of immersion.

sandwich with pure composite faces caused a remarkable decrease in natural frequency, which decreases 15.23 %, 6.79 %, 4.64 %, 3.37 %, 3.06 %, and 2.72 % in modes 1 to 6, respectively.

As depicted in Fig. 7(a), the frequencies of modes 1 to 6 of the sandwich plate with a reinforced GFRP face containing 3 wt% of nanosilica exhibit reductions of 13.72 %, 7.93 %, 6.22 %, 5.22 %, 5.08 %, and 4.60 % after one month of immersion. Similarly, for the sandwich plate with the face reinforced by 3 wt% of nanoclay, the frequencies of modes 1 to 6 have decreased by 12.64 %, 5.60 %, 4.21 %, 3.04 %, 2.29 %, and 2.62 %, respectively, during the one-month immersion period (see Fig. 7(b)).

According to the results of Figs. 6 and 7, the sandwich plate with GFRP faces reinforced by 3 wt% of nanoclay has the lowest frequency reduction for each mode shape and gives more stability to the sandwich structure during immersion in sulfuric acid. The diagram of Fig. 8 compares the forced frequency of sandwich plates after one month of acid immersion.

Considering $\beta^{acid}$ and higher swelling of pure GFRP faces, the lowest frequency under environment pre-stress is related to the sandwich with the neat face. On the other hand, according to Fig. 2, adding nanoparticles to the layers of sandwich structures has caused less longitudinal expansion and better durability that increased the frequency of sandwich.

It can be seen in Fig. 8, adding 3 wt% of nanoclay or nanosilica to the faces of the sandwich plate causes less frequency reduction

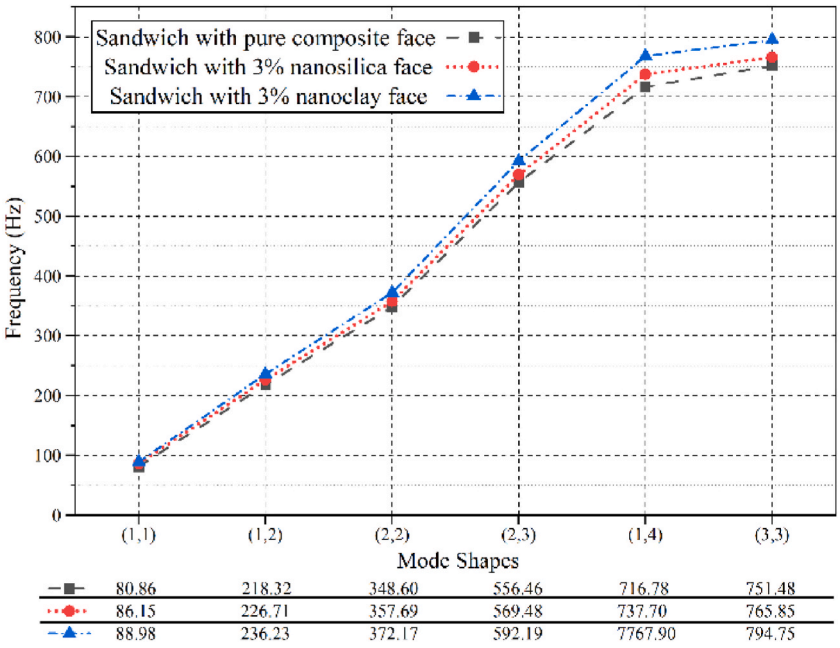


**Fig. 8.** The comparisons of frequency of forced vibration for sandwich after one month of immerision in the acid.

and 10.04 % and 6.54 % improvement, respectively, in the first frequency mode during a month-long of submerging in the sulfuric acid.

As obtained results show, reinforcing sandwich plates with nanoparticles prevents the destruction of the acidic environment and improves the frequency; Also, it can be stated that adding 3 wt% of nanoclay to the composite faces of the sandwich plate had a better effect on the vibration frequency.

## 5. Conclusion

A comprehensive investigation was carried out to analyze the vibrations of a sandwich plate with GFRP faces, which were strengthened with a composite material comprising 3 wt% of nanoparticles. The study focused on evaluating the impact of these nanoparticles on the mechanical properties and frequency characteristics of both the faces and the overall sandwich plate. Vibrations of the sandwich plate were analyzed with the LOPSDT, and the natural frequency was validated with the results of the ANSYS numerical solution. The frequency results for six modes of free vibrations and vibrations under environmental load conditions were obtained for a sandwich plate. Subsequently, the effectiveness of incorporating clay and silica nanoparticles into the composite faces was assessed and compared. Based on obtained results, some conclusions are as follows:

- The incorporation of 3 wt% of silica and clay nanoparticles into the composite faces resulted in a substantial increase in the tensile modulus compared to the pure specimens. Specifically, the tensile modulus exhibited a rise of 24.84 % and 32.52 % for the nanosilica and nanoclay reinforced composites, respectively. Furthermore, even after a month-long immersion in sulfuric acid, the tensile modulus of the nanosilica and nanoclay reinforced GFRP composites remained 12.07 % and 36.81 % higher, respectively, than that of the pure specimens, despite experiencing a decrease.
- Adding 3 wt% of nanoclay causes better resistance of the GFRP composite in the sulfuric acid, and the composite with 3 wt% nanoclay will have less longitudinal and mass changes than other specimens in acid.
- During the analysis of free vibrations in a sandwich plate, it was observed that the natural frequency of the first mode increased by 6.81 % and 4.66 % for the sandwich plate with GFRP faces reinforced by 3 wt% of nanosilica and nanoclay, respectively. However, after undergoing a month-long immersion, the natural frequency of the sandwich plate with pure composite layers and GFRP faces containing 3 wt% of nanoclay experienced a decrease of approximately 1 %. Conversely, the sandwich plate with GFRP faces reinforced by 3 wt% of nanosilica exhibited a higher reduction of over 3 % in its natural frequency.
- Studying the forced vibrations under pre-stress of an acidic environment showed that adding 3 wt% of nanoclay and nanosilica to the GFRP faces of the sandwich plate has caused a lower frequency reduction and 10.04 % and 6.54 % improvement in the frequency of the first mode, compared to the sandwich with pure GFRP faces after a month-long of submerging in the sulfuric acid.
- The results illustrated better effects of adding 3 wt% of nanoclay on the mechanical properties of GFRP composite face and improving the vibration frequency of sandwich plates with the GFRP faces reinforced with 3 wt% nanoclay in the sulfuric acid environment.

## Availability of data and materials

All the datasets necessary to support the conclusions drawn in this study are provided within the article.

## CRediT authorship contribution statement

**Farshad Rahmani:** Conceptualization, Data curation, Investigation, Methodology, Software, Validation, Writing – original draft. **Reza Barbaz-Isfahani:** Conceptualization, Investigation, Methodology, Supervision, Validation, Writing – original draft. **Saeed Saber-Samandari:** Conceptualization, Investigation, Project administration, Supervision, Validation, Writing – review & editing. **Manouchehr Salehi:** Conceptualization, Project administration, Supervision, Validation, Writing – review & editing.

## Declaration of competing interest

The authors declare that they have no known competing financial interests or personal relationships that could have appeared to influence the work reported in this paper.

## References

[1] Zhen Huo, Mohaned Mohamed, J.R. Nicholas, Sudharshan Anandan, K. Chandrashekhara, Effect of salt water exposure on foam-cored polyurethane sandwich composites, J. Sandw. Struct. Mater. 22 (2020) 1256–1273.
[2] Karthik Ram Ramakrishnan, Sandra Guérard, Zhifang Zhang, Krishna Shankar, P. Viot, Numerical modelling of foam-core sandwich panels with nano-reinforced composite facesheets, J. Sandw. Struct. Mater. 23 (2021) 1166–1191.
[3] L.-M. Tian, B.-B. Jin, L. Li, Axial compressive mechanical behaviors of a double-layer member, J. Struct. Eng. 149 (2023), 04023110.
[4] Y. Zhao, J. Jing, L. Chen, F. Xu, H. Hou, Current research status of interface of ceramic-metal laminated composite material for armor protection, Acta Metall. Sin. 57 (2021) 1107–1125.
[5] Daniel A. Drake, Rani W. Sullivan, Stephen Clay, On the use of a trilinear traction-separation law to represent stitch failure in stitched sandwich composites, J. Sandw. Struct. Mater. 24 (2022) 1367–1384.
[6] J. Li, M. Chen, Z. Li, Improved soil–structure interaction model considering time-lag effect, Comput. Geotech. 148 (2022), 104835.
[7] H. He, E. Shuang, L. Ai, X. Wang, J. Yao, C. He, B. Cheng, Exploiting machine learning for controlled synthesis of carbon dots-based corrosion inhibitors, J. Clean. Prod. 419 (2023), 138210.
[8] Q. Fu, K. Luo, Y. Song, M. Zhang, S. Zhang, J. Zhan, J. Duan, Y. Li, Study of sea fog environment polarization transmission characteristics, Appl. Sci. 12 (2022) 8892.
[9] H. Li, S. Si, K. Yang, Z. Mao, Y. Sun, X. Cao, H. Yu, J. Zhang, C. Ding, H. Liang, Hexafluoroisopropanol based silk fibroin coatings on AZ31 biometals with enhanced adhesion, corrosion resistance and biocompatibility, Prog. Org. Coating 184 (2023), 107881.
[10] Z. Fu, B. Yang, M. Shan, T. Li, Z. Zhu, C. Ma, X. Zhang, G. Gou, Z. Wang, W. Gao, Hydrogen embrittlement behavior of SUS301L-MT stainless steel laser-arc hybrid welded joint localized zones, Corrosion Sci. 164 (2020), 108337.
[11] W. Zhang, S. Kang, X. Liu, B. Lin, Y. Huang, Experimental study of a composite beam externally bonded with a carbon fiber-reinforced plastic plate, J. Build. Eng. 71 (2023), 106522.
[12] C. Liu, J. Cui, Z. Zhang, H. Liu, X. Huang, C. Zhang, The role of TBM asymmetric tail-grouting on surface settlement in coarse-grained soils of urban area: field tests and FEA modelling, Tunn. Undergr. Space Technol. 111 (2021), 103857.
[13] Z. Dai, J. Xie, M. Jiang, A coupled peridynamics–smoothed particle hydrodynamics model for fracture analysis of fluid–structure interactions, Ocean Eng. 279 (2023), 114582.
[14] K. Yang, N. Qin, H. Yu, C. Zhou, H. Deng, W. Tian, S. Cai, Z. Wu, J. Guan, Correlating multi-scale structure characteristics to mechanical behavior of Caprinae horn sheaths, J. Mater. Res. Technol. 21 (2022) 2191–2202.
[15] X. Bai, H. Shi, K. Zhang, X. Zhang, Y. Wu, Effect of the fit clearance between ceramic outer ring and steel pedestal on the sound radiation of full ceramic ball bearing system, J. Sound Vib. 529 (2022), 116967.
[16] H. Lu, Y. Zhu, M. Yin, G. Yin, L. Xie, Multimodal fusion convolutional neural network with cross-attention mechanism for internal defect detection of magnetic tile, IEEE Access 10 (2022) 60876–60886.
[17] J. Shi, B. Zhao, T. He, L. Tu, X. Lu, H. Xu, Tribology and dynamic characteristics of textured journal-thrust coupled bearing considering thermal and pressure coupled effects, Tribol. Int. 180 (2023), 108292.
[18] L.-m. Tian, M.-h. Li, L. Li, D.-y. Li, C. Bai, Novel joint for improving the collapse resistance of steel frame structures in column-loss scenarios, Thin-Walled Struct. 182 (2023), 110219.
[19] Y.-y. Wang, M. Lou, Y. Wang, W.-g. Wu, F. Yang, Stochastic failure analysis of reinforced thermoplastic pipes under axial loading and internal pressure, China Ocean Eng. 36 (2022) 614–628.
[20] R.-B. Hao, Z.-Q. Lu, H. Ding, L.-Q. Chen, Orthogonal six-DOFs vibration isolation with tunable high-static-low-dynamic stiffness: experiment and analysis, Int. J. Mech. Sci. 222 (2022), 107237.
[21] S. Narayanan, M.N. Hegde, S. Thirunarayanan, T.S. Dsouza, Fracture resistance of teeth restored with newer methacrylate-based dental composite materials: an in vitro study, Dent. Hypotheses 13 (2022).
[22] W.S. Salloom, B. Shukri, Effects of chitosan, NaOCl, and EDTA irrigation solutions on the cyclic fatigue resistance of three nickel–titanium endodontic rotary files: an in vitro study, Dent. Hypotheses 13 (2022).
[23] S.M. Zaidan, R. Rafeeq, Comparison of shear bond strength of three luting materials used in band and loop space maintainer cementation: an in vitro study, Dent. Hypotheses 13 (2022) 136.
[24] M. Hoseini, M.R. Malekipour, F. Shirani, The effect of application of sonic vibration on the bond strength of glass fiber post to root dentin using duo-link and theracem cements: an in vitro study, Dent. Hypotheses 13 (2022).
[25] Y. Gong, Z.-G. Yang, Corrosion evaluation of one wet desulfurization equipment–Flue gas desulfurization unit, Fuel Process. Technol. 181 (2018) 279–293.
[26] D. Le, W. Ji, J. Kim, K. Jeong, S. Lee, Effect of antimony on the corrosion behavior of low-alloy steel for flue gas desulfurization system, Corrosion Sci. 50 (2008) 1195–1204.
[27] H.H. Jasim, M.K. Gholam, B. Shukri, Assessment of the shear bond strength of composite resin to fresh amalgam using different adhesion protocols: an in vitro study, Dent. Hypotheses 13 (2022).
[28] H.A. Saleh, O.H. Abdulhameed, A comparative examination of cyclic fatigue and fragment length of three different types of endodontic rotary files: an in vitro study, Dent. Hypotheses 13 (2022) 49.
[29] Lei Wang, Ke Wang, Ling Chen, Yongwei Zhang, Chaobin He, Preparation, morphology and thermal/mechanical properties of epoxy/nanoclay composite, Composites Part A 37 (2005) 1890–1896.

[30] Ali Asghar Jahangiri, Rostamiyan Yasser, Mechanical properties of nano-silica and nano-clay composites of phenol formaldehyde short carbon fiber, J. Compos. Mater. 0 (2019) 1–14.
[31] M. Somaiah, Chowdary, M.S.R Niranjan Kumar, Effect of nanoclay on the mechanical properties of polyester and S-glass fiber (Al), International Journal of Advanced Science and Technology 74 (2015) 35–42.
[32] A. Bledzki, R. Spaude, G.W. Ehrenstein, Corrosion phenomena in glass fibers and glass fiber reinforced thermosetting resins, Compos. Sci. Technol. 23 (1985) 263–285.
[33] Mahdi Heydari-Meybodi, Saeed Saber-Samandari, Mojtaba Sadighi, A new approach for prediction of elastic modulus of polymer/nanoclay composites by considering interfacial debonding: experimental and numerical investigations, Compos. Sci. Technol. 117 (2015) 379–385.
[34] S.H.T. Mahmoud K. Mahmoud, Effect of strong acids on mechanical properties of glass/polyester GRP pipe at normal and high temperatures, Polym. Plast. Technol. Eng. 42 (2003) 677–688.
[35] Saeed Saber-Samandari, Akbar Afaghi Khatibi, Domagoj Basic an experimental study on clay/epoxy nanocomposites produced in a centrifuge, Compos. B Eng. 38 (2007) 102–107.
[36] M. Stamenovic, S. Putic, M. Rakin, B. Medjo, D. Cikara, Effect of alkaline and acid solutions on the tensile properties of glass-polyester pipes, Mater. Des. 32 (2011).
[37] Hamza M. Kamal, Mohammed J. Kadhim, Effect of chemical solutions on the mechanical properties of nano-silica reinforced (glass/Kevlar) fabrics polyester hybrid composite materials, Int. J. Energy Environ. 9 (2018) 187–194.
[38] A. Hammami, N. Al-ghuilani, Durability and environmental degradation of glass-vinylester composites, Polym. Compos. 25 (2004) 609–616.
[39] Jonathon D. Tanks, Yoshihiko Arao, Masatoshi Kubouchi, Diffusion kinetics, swelling, and degradation of corrosion-resistant C-glass/epoxy woven composites in harsh environments, Compos. Struct. 202 (2018) 686–694.
[40] P. Rama Subba Reddy, T. Sreekantha Reddy, I. Srikanth, P. Ghosal, V. Madhu, K. Venkateswara Rao, Influence of nanoclay and incident energy on impact resistance of S2-glass/epoxy composite laminates subjected to low velocity impact, Adv. Mater. Lett. 8 (2017) 174–179.
[41] Su Chang, Xin Wang, Lining Ding, Zhishen Wu, Enhancement of mechanical behavior of FRP composites modified by silica nanoparticles, Construct. Build. Mater. (2020) 262.
[42] R. Barbaz-Isfahani, H. Dadras, A. Taherzadeh-Fard, M.A. Zarezadeh-Mehrizi, S. Saber-Samandari, M. Salehi, G. Liaghat, Synergistic effects of incorporating various types of nanoparticles on tensile, flexural, and quasi-static behaviors of GFRP composites, Fibers Polym. 23 (2022) 2003–2016.
[43] H. Dadras, R. Barbaz-Isfahani, S. Saber-Samandari, M. Salehi, Experimental and multi-scale finite element modeling for evaluating healing efficiency of electro-sprayed microcapsule based glass fiber-reinforced polymer composites, Polym. Compos. 43 (2022) 5929–5945.
[44] H. Khorshidi, C. Zhang, E. Najafi, M. Ghasemi, Fresh, mechanical and microstructural properties of alkali-activated composites incorporating nanomaterials: a comprehensive review, J. Clean. Prod. (2022), 135390.
[45] R. Barbaz-Isfahani, S. Saber-Samandari, M. Salehi, Multi-scale modeling and experimental study on electrosprayed multicore microcapsule-based self-healing polymers, Mech. Adv. Mater. Struct. (2022) 1–14.
[46] M. Safaei, R. Abedinzadeh, A. Khandan, R. Barbaz-Isfahani, D. Toghraie, Synergistic effect of graphene nanosheets and copper oxide nanoparticles on mechanical and thermal properties of composites: experimental and simulation investigations, Mater. Sci. Eng., B 289 (2023), 116248.
[47] A. Teimouri, R. Barbaz Isfahani, S. Saber-Samandari, M. Salehi, Experimental and numerical investigation on the effect of core-shell microcapsule sizes on mechanical properties of microcapsule-based polymers, J. Compos. Mater. 56 (2022) 2879–2894.
[48] R. Barbaz-Isfahani, H. Dadras, S. Saber-Samandari, A. Taherzadeh-Fard, G. Liaghat, A comprehensive investigation of the low-velocity impact response of enhanced GFRP composites with single and hybrid loading of various types of nanoparticles, Heliyon 9 (2023).
[49] R. Barbaz-Isfahani, A. Khalvandi, T.M.N. Tran, S. Kamarian, S. Saber-Samandari, J.-i. Song, Synergistic effects of egg shell powder and halloysite clay nanotubes on the thermal and mechanical properties of abacá/polypropylene composites, Ind. Crop. Prod. 205 (2023), 117498.
[50] D.J. Kadhem, A. Al Haidar, Remineralization of dentine caries using moringa oleifera based nano-silver fluoride: a single-blinded, randomized, active-controlled clinical trial, Dent. Hypotheses 13 (2022) 82–85.
[51] H.T. Zedan, Z.J. Jafar, A comparison of solubility among zinc oxide Eucalyptus and zinc oxide eugenol: an in vitro study, Dent. Hypotheses 13 (2022) 142.
[52] M. Alsaadi, M. Bulut, A. Erkliğ, A. Jabbar, Nano-silica inclusion effects on mechanical and dynamic behavior of fiber reinforced carbon/Kevlar with epoxy resin hybrid composites, Compos. B Eng. 152 (2018) 169–179.
[53] C. Senthamaraikannan, R. Ramesh, Evaluation of mechanical and vibration behavior of hybrid epoxy carbon composite beam carrying micron-sized CTBN rubber and nanosilica particles, Proc. Inst. Mech. Eng., Part L 233 (2019) 1738–1752.
[54] Wiwat Keyoonwong, Yi Guo, Masatoshi Kubouchi, Saiko Aoki, Tetsuya Sakai, Corrosion behavior of three nanoclay dispersion methods of epoxy/organoclay nanocomposites, International Journal of Corrosion 2012 (2012) 1–11.
[55] Yasaman Gitiara, Reza Barbaz-Isfahani, Saeed Saber-Samandari, Mojtaba Sadighi, Low-velocity impact behavior of incorporated GFRP composites with nanoclay and nanosilica in a corrosive environment: experimental and numerical study, J. Compos. Mater. 0 (2021) 1–22.
[56] Xiangyang Li, Kaiping Yu, Jingyong Han, Rui Zhao, Ying Wu, A piecewise shear deformation theory for free vibration of composite and sandwich panels, Compos. Struct. 124 (2015) 111–119.
[57] Xiangyang Li, Kaiping Yu, Rui Zhao, Thermal post-buckling and vibration analysis of a symmetric sandwich beam with clamped and simply supported boundary conditions, Arch. Appl. Mech. 88 (2017) 543–561.
[58] Rui Zhao, Kaiping Yu, M. Gregory, Hulbert, Ying Wu, Xiangyang Li, Piecewise shear deformation theory and finite element formulation for vibration analysis of laminated composite and sandwich plates in thermal environments, Compos. Struct. 160 (2017) 1060–1083.
[59] Xiangyang Li, Kaiping Yu, Vibration and acoustic responses of composite and sandwich panels nder thermal environment, Compos. Struct. 131 (2015) 1040–1049.
[60] H. Dadras, A. Teimouri, R. Barbaz-Isfahani, S. Saber-Samandari, Indentation, finite element modeling and artificial neural network studies on mechanical behavior of GFRP composites in an acidic environment, J. Mater. Res. Technol. 24 (2023) 5042–5058.
[61] M. Heydari-Meybodi, S. Saber-Samandari, M. Sadighi, An experimental study on low-velocity impact response of nanocomposite beams reinforced with nanoclay, Compos. Sci. Technol. 133 (2016) 70–78.
[62] R.M. Monfared, M.R. Ayatollahi, R.B. Isfahani, Synergistic effects of hybrid MWCNT/nanosilica on the tensile and tribological properties of woven carbon fabric epoxy composites, Theor. Appl. Fract. Mech. 96 (2018) 272–284.
[63] R. Barbaz-Isfahani, S. Saber-Samandari, M. Salehi, Novel electrosprayed enhanced microcapsules with different nanoparticles containing healing agents in a single multicore microcapsule, Int. J. Biol. Macromol. 200 (2022) 532–542.
[64] R. Barbaz-Isfahani, S. Saber-Samandari, M. Salehi, Experimental and numerical research on healing performance of reinforced microcapsule-based self-healing polymers using nanoparticles, J. Reinforc. Plast. Compos. (2022), 07316844221102945.
[65] M.A. Maghsoudlou, R. Barbaz Isfahani, S. Saber-Samandari, M. Sadighi, The response of GFRP nanocomposites reinforced with functionalized SWCNT under low velocity impact: experimental and LS-DYNA simulation investigations, Iranian Journal of Materials Science and Engineering 18 (2021).
[66] ASTM Standard C581 ,Standard Practice for Determining Chemical Resistance of Thermosetting Resins Used in Glass-Fiber-Reinforced Structures Intended for Liquid Service.
[67] ASTM, Standard D5229/D5229M, Standard Test Method for Moisture Absorption Properties and Equilibrium Conditioning of Polymer Matrix Composite Materials, 2004.
[68] ASTM Standard D3039/D3039M, Standard Test Method for Tensile Properties of Polymer Matrix Composite Materials.
[69] ASTM, Standard D3518/D3518M, Standard Test Method for In-Plane Shear Response of Polymer Matrix Composite Materials by Tensile Test of a (+/-)45° Laminate, 2007.
[70] Methods for Determining the Density of Non-cellular Plastics, 2004.

[71] G. Romeo, E. Miraldi, G. Ruscica, F. Berroglion, G. Ruvinetti, A new test facility designed to measure the coefficient of moisture expansion of advanced composites, J. Compos. Technol. Res. 14 (1992) 225–230.
[72] A. Poenninger, B. Defoort, Determining the coefficient of moisture expansion (CME), Proceedings of the 9th International Symposium on Materials in a Space Environment (2003) 567–572.
[73] F. Rahmani, R. Barbaz-Isfahani, S. Saber-Samandari, M. Salehi, Effect of corrosive environment on mechanical properties of polymer-based nanocomposite: analytical and experimental study, Mater. Today Commun. 36 (2023), 106544.
[74] J.N. Reddy, Mechanics of Laminated Composite Plates and Shells: Theory and Analysis, 2003, pp. 81–85.
[75] S. Brischetto, Hygrothermoelastic analysis of multilayered composite and sandwich shells, J. Sandw. Struct. Mater. 15 (2013) 168–202.